Finding the best exoplanets to search for exomoons by radial velocity

Author: Ioannis Koutalios
Supervisor: Matthew Kenworthy

THESIS
submitted in partial fulfilment of the
requirements for the degree of
MASTER OF SCIENCE
in
ASTRONOMY

Leiden, The Netherlands

January 11, 2023

Abstract

Observing an exomoon around exoplanets by using radial velocity data from the host planet has proven to be a demanding task. We explore the possibilities for such a discovery and the limitations posed by our current technology. Our main focus is on the exoplanet β Pictoris b, which has proven to be a great candidate due to its mass and orbital inclination. We analyze a technique for measuring radial velocities by using the cross-correlation of spectra. We then simulate the process of an exomoon detection and propose possible future observations that would allow us to achieve one. Lastly, we focus on two sets of radial velocity data for β Pictoris b, which we attempt to link to the possible existence of spots on the planet's atmosphere.

Acknowledgements

I would like to thank my supervisor, professor Matthew Kenworthy for his guidance during this project. He showed me great trust, which enabled me to work in this fascinating field and produce this work. I also want to thank his team of PhD students for our collaboration and for welcoming me to their team. Especially I want to thank Rico Landmann for all our private communications and for providing me with the radial velocity data used during this project. The two spectra were provided by Dr Tomas Stolker and Dr Paul Mollière, so I take this chance to express my gratitude to them as well.

My family and friends have supported me for all these years and I wouldn't be here without them. I want to thank them for all the love they showed me. Last but not least, this endeavour would not have been possible without the love and emotional support I got from my girlfriend Polina.

Contents

Chapter 1

Introduction

1.1 Exoplanets

The search for exoplanets is one of modern astronomy's most exciting and ambitious endeavours. It has enabled us to delve into the depths of our universe and discover planets outside of our own solar system. Thousands of exoplanets have been discovered, and each new one brings us one step closer to understanding our cosmic neighbourhood.

The very first exoplanet to be discovered was in fact two planets orbiting the PSR 1257+12 pulsar (Wolszczan et al., 1992). Scientists were able to detect them by accurately measuring the pulses of the star using data collected from the Arecibo radiotelescope. In 2020, the first potentially habitable exoplanet was discovered (Gilbert et al., 2020) orbiting the star TOI 700. Studying the exoplanets can provide valuable insight into the formation of our own solar system and the life cycle of stars.

In recent years our understanding of exoplanets has been revolutionized by the development of sophisticated techniques for their discovery. These techniques make it easier than ever to detect planets orbiting distant stars, and in turn, understand the processes that form solar systems. Transit photometry, radial velocity, microlensing, and direct imaging are among the most successful methods used to detect exoplanets, while other techniques are gaining traction. Each of these methods has its own advantages and disadvantages and provides unique insight into the formation of exoplanetary systems.

The method of direct imaging is relatively new compared to the other ones. The first planet to be discovered using this technique was the planet 2M1207b which is orbiting around a brown dwarf (Chauvin et al., 2004; Mohanty et al., 2007). Observations of exoplanets through direct imaging have

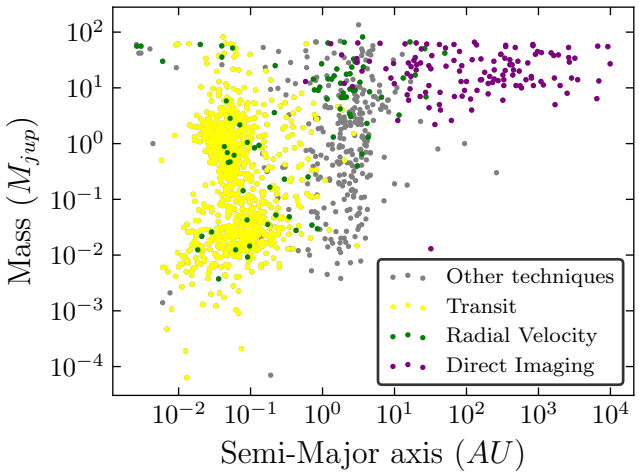

Figure 1.1: All the discovered exoplanets with known mass and semi-major axis of their orbit. The colours represent the different techniques that were used to detect them. Data was obtained from exoplanets.eu (Exoplanet Team, n.d.).

many advantages as it allows scientists to analyze the spectrum produced by the planet and directly measure the elements that are present in its atmosphere. This method also allows the observation of planets at a greater distance from the host star compared to the other methods. This effect becomes clear by looking at Figure 1.1.

Telescopes both in space and on Earth have been used to capture direct images of exoplanets, helping to unlock their secrets and giving us a better understanding of the universe. By studying the light signatures of these planets, astronomers can learn more about their atmospheres, orbits, sizes, and compositions. In addition, direct imaging data can be used to test current theories of planetary formation and evolution in order to develop new models.

The mass and composition of the exoplanet play a significant role in the potential habitability of the exoplanet. Although potential life in gas planets can not be eliminated, scientists are currently focusing on rocky planets with atmospheres. The planet's atmosphere, surface temperature, and distance from its parent star as well as the mass greatly influence the exoplanet's habitability.

The discussion for habitability should also include potential moons around exoplanets. This opens the door to many more potential worlds where life could evolve, including moons around gas giants like most of the exoplanets that have already been discovered.

1.2 Exomoons

An extrasolar moon is a natural satellite around an exoplanet and it is usually referred to as an exomoon. Based on our own solar system exomoons should be frequent, especially around gas giant planets like most of the exoplanets that have been discovered. However, detecting them can be challenging because they are much smaller than their host planets.

The formation of moons is a question that has been around for many years. It is not yet clear how our own moon has been created and there are many theories (René Heller, 2020) as to how multiple moon systems around gas giants can be formed. All these theories greatly depend on the characteristics of the host planet. Also, different moons can be formed through different processes or even a combination of them.

One of the main theories is that moons form from the debris that is left over after the creation of the planet (Alibert et al., 2005). This theory is able to explain the formation of a single moon as well as multiple moons, as observed at the gas giants of our solar system. It is also possible that planets can capture small objects with their gravitational field and keep them in orbit. Lastly, when two objects collide, especially in the early stages of the formation of the planetary system, the leftover object can be captured by the planet and form a moon.

As has already been mentioned, detecting exomoons is not an easy task. There are many different techniques that have been suggested for exomoon detection. According to René Heller (2020) there are three categories. The first is "Dynamical Effects on Planetary Transits", which includes the "Transit Timing Variation"(David M. Kipping, 2009a) and "Transit Duration Variation"(David M. Kipping, 2009b), meaning that the potential moon impacts either when the planet will transit the host star, or how long will the transit last.

The second category is "Direct Transit Signatures of Exomoons" which includes techniques that measure the direct transit of the exomoon on the host star. As the exoplanet transits the host star, the exomoon will also contribute to the measured light curve. Depending on the position of the moon at the time of the transit it can have an impact at the beginning or the end of the curve.

A third category can be made for exoplanets that can be observed using direct imaging techniques. For these planets, we can search for exomoons by measuring the effects of the moon directly on the planet that it orbits. This effect can be either a transit of the moon in front of the planet (R. Heller, 2016) or, as we explore in this project, the measured radial velocity of the planet.

There are currently many exoplanets for which we have strong indications of potential exomoons orbiting around them. Using many different methods scientists have declared many exomoon candidates in the last few years. Two of the most notable cases are Kepler-1625 b-i and Kepler-1708 b-i. The first was announced by Teachey et al. (2018) based on three separate transits between 2009 and 2013, using data from the Kepler telescope. In D. Kipping et al. (2022), the team created a survey of 70 cool giants (gas giants at a great distance from the host star) and announced a new exomoon candidate in Kepler-1708 b-i. The survey also made use of data collected by the Kepler telescope.

The habitability of exomoons is similar to the one for exoplanets. The exomoon can be heated in various ways. The first is the reflected starlight as described in the paper René Heller et al. (2013). In the same paper, they also discuss tidal heating as another method for an energy source. Finally, there is also thermal irradiation from the host planet to the exomoon, which can also affect the potential habitability of the moon (R. Heller et al., 2015).

1.3 β Pictoris b

The young star Beta Pictoris (β Pic) debris disk was discovered in 1984, sparking curiosity in the region, that eventually led to further investigations and the 2008 finding of the gas giant exoplanet β Pic b (Bonnefoy et al., 2014; Chauvin et al., 2012). The planet was the closest direct imaged exoplanet to a host star at the time, with a semi-major axis in the $(8-9)$ AU range near the time of its discovery. The orbit is currently restricted to an orbital semi-major axis of $9.93 \pm 0.03 AU$.

The K-band spectro-interferometric observations from the GRAVITY instrument of the VLT, combined with new astrometry and Hipparcos/Gaia data, indicated a mass of $12.7 \pm 2.2 M_{Jup}$ (GRAVITY Collaboration et al., 2020), in agreement with the earlier mass determinations. Even if the numbers for the orbital eccentricity seem to be more dispersed, the values of $0.12^{+0.04}_{-0.03}$ (Nielsen et al., 2020), $0.15^{+0.05}_{-0.04}$ (GRAVITY Collaboration et al., 2020) concur in favour of a non-circular orbit, which is unusual for a planet of this size but can be explained by the presence of another giant planet in the system. Eccentricity is reported to be $0.01^{+0.029}_{-0.01}$ by VLT/SPHERE data post conjunction (Lagrange et al., 2019).

The radius of the planet was measured in Currie et al. (2013). They used cutting-edge image processing techniques to evaluate fresh and old VLT and Gemini high-contrast images of the planet in seven near-to-mid IR photometric filters in order to provide measurements with a high signal-to-noise

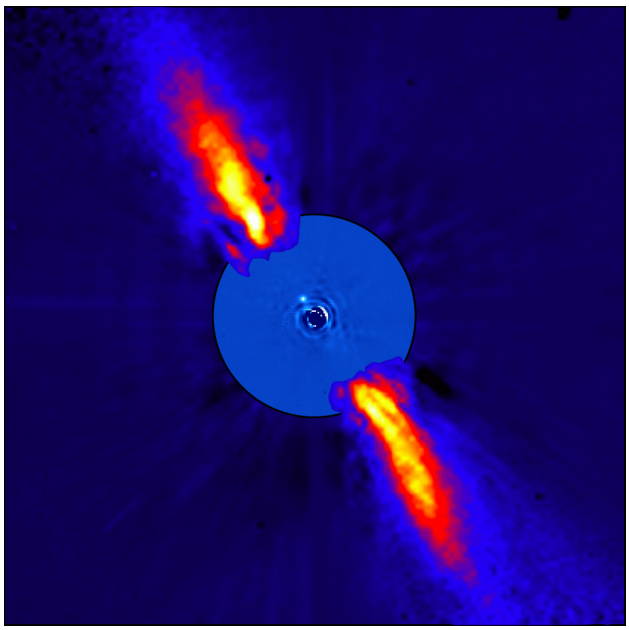

Figure 1.2: Beta Pictoris' close environment as seen in near-infrared light. The outer part of the image depicts the reflected light on the dust disc, as seen in 1996 with the ADONIS instrument on ESO's 3.6 m telescope; the inner part depicts the system's innermost part, as seen at 3.6 microns with NACO on the Very Large Telescope. The planet Beta Pictoris b can be seen as a white spot orbiting around the centre of the dark disk, which is used to hide the luminosity of the star. Image taken from the ESO public library (European South Observatory, n.d.).

ratio. The results gave us a radius of $1.65 \pm 0.06 R_{Jup}$

In a more recent paper (Lacour et al., 2021) researchers used a two-planet model in order to determine the parameters of β Pic b alongside the newly discovered β Pic c. They combined earlier astrometry of β Pic b with fresh GRAVITY interferometer observations. Using Markov chain Monte Carlo simulations in Jacobi coordinates, the orbital motion of β Pic b was fitted. The final mass that was calculated is $11.90^{+2.93}_{-3.04} M_{Jup}$.

During this project, we mainly focused on the planet β Pictoris b, because it meets all the criteria to make such a detection possible. It is an easily observable (using direct imaging) exoplanet with an edge-on orbit. We also have in mind the possibility of being granted observational time from the Crires+[1] in the near future, to obtain enough radial velocity data on β Pictoris b, to either make a detection or lower the threshold for potential

[1]European Southern Observatory, n.d.(a).

exomoons around the planet.

In Chapter 2 we will discuss the radial velocity impact of moons on the host planet by using both the example of Jupiter and β Pictoris b. Then in Chapter 3 we will use two simulated spectra, in order to simulate and measure a Doppler shift. After that, in Chapter 4, we will simulate the whole process of exomoon detection in β Pictoris b by generating radial velocity signals and measuring the parameters of the exomoon orbit, using a full Bayesian model. The results will give us the expected thresholds of detections of that nature. Finally, in Chapter 5 we will attempt to explain some real radial velocity signals for β Pictoris b, obtained by two one-hour-long observational runs. To achieve that we will simulate spots on the atmosphere of β Pictoris b and analyze the radial velocity signals they produce.

Chapter 2

Radial velocity of moons around β Pic b

2.1 Methods

In this chapter, we will explore the radial velocities of potential moons around the planet β Pictoris b. The parameters we use during this analysis are given in Table 2.1. At the time of writing these are considered to be the best estimations (Lacour et al., 2021; Currie et al., 2013; Exoplanet Team, n.d.).

Mass (M_j)	Radius (R_j)
11.9	1.65

Table 2.1: The parameters of β Pic b used in this project. Both the mass and the radius of the planet are given in Jupiter units.

As a reference point, we will use the moon of Jupiter, Io, and the effects it has on the planet. The parameters of Io are given in Table 2.2.

Mass ($M_\oplus$)	Radius ($R_\oplus$)	Period (days)
0.01495	0.286	1.769

Table 2.2: The parameters of Io used in this project. Both the mass and the radius of the moon are given in Earth units.

The analysis was done using the exoplanet module (Foreman-Mackey, Rodrigo Luger, et al., 2021a; Foreman-Mackey, Savel, et al., 2021; Foreman-

Mackey, Rodrigo Luger, et al., 2021b) and its dependencies (Agol et al., 2020; Kumar et al., 2019; Astropy Collaboration et al., 2013; Astropy Collaboration et al., 2018; D. M. Kipping, 2013; R. Luger et al., 2019; Salvatier et al., 2016a; Theano Development Team, 2016). Originally it was designed to simulate the orbits of exoplanets around their host star and generate the position and velocities of both the host star and the exoplanet as a function of time. We can however use a planet as the main body and the moon as the secondary object by giving the correct parameters when calling the module. We can then generate the data for the radial velocity of the star, which in our case will be the planet.

We chose to simulate an exomoon around β Pic b that has the mass of the Earth and a period of 10 days. This starting point was chosen in order to give us an indication of the scale of radial velocities we should expect to get. The case of Jupiter and Io was also used as an example within our own solar system. For all the cases we assumed an inclination of $i = 90$ between the normal to orbital plane and line of sight. We also assumed that the orbits are circular, which we know is not true for Io ($e = 0.004$) but is a good approximation and helps us be consistent when comparing it to our exomoon example.

After that, we implemented many more simulations in order to get the peaks of the radial velocity for each one. By looping over all the different orbital periods we expect to be able to observe we get a picture of how the radial velocity declines with respect to that. We also loop over the different masses to visualise the effect of it on the radial velocity. As we are doing this we are essentially mapping the peak radial velocity for all the different cases that seem realistic for our scenario.

2.2 Results

The radial velocity caused by Io on Jupiter and the effect of a potential Earth-mass exomoon around β Pic b are shown in Figure 2.1

The period of Io is much shorter compared to the potential exomoon that we defined to have a period of 10 days and this is reflected in how many peeks we get over the same period of time.

What is more interesting is the amplitude of the radial velocities for both cases. Io has a much smaller effect on Jupiter compared to the potential exomoon on β Pic b.

We can derive an approximate formula for the radial velocity of the planet that is caused by the moon if we assume 90° inclination between the normal to the orbital plane and the line of sight, as well as a circular orbit.

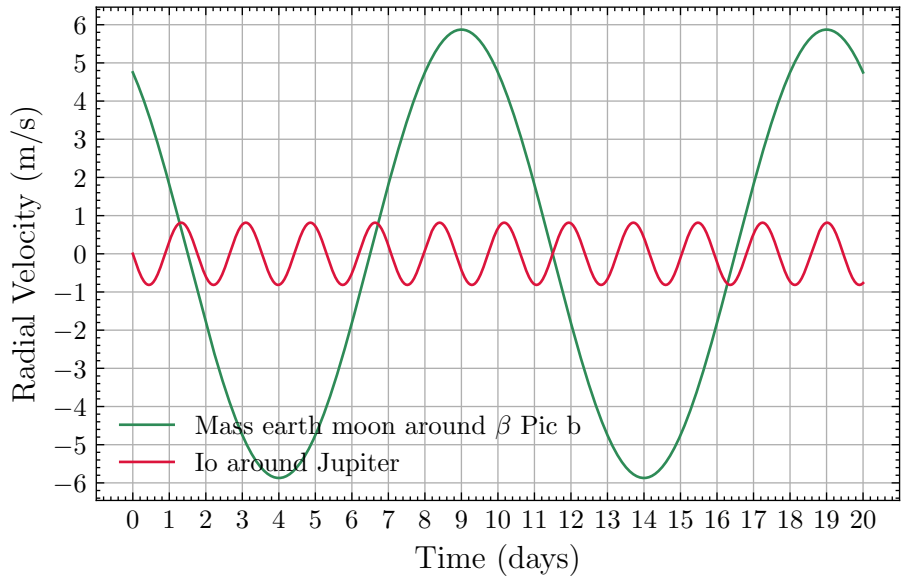

Figure 2.1: The radial velocities of Jupiter (red) and β Pic b (green) that are caused by Io and a potential Earth-mass exomoon respectively as a function of time. The radial velocity is measured in (m/s) while the time is measured in days.

From the conservation of momentum we have

$$Mv_{planet} = mv_{moon} \tag{2.1}$$

where M is the mass of the planet and m is the one of the moon.

From the circular motion, we get

$$v_{moon} = \frac{2\pi a}{P} \tag{2.2}$$

where a is the semi-major axis or in our case, the radius of the circular orbit, and P is the period

From Kepler's third law with the assumption that $m << M$

$$\frac{a^3}{P^2} = \frac{GM}{4\pi^2} \tag{2.3}$$

When we combine Equations (2.1) to (2.3) we get

$$v_{planet} = \left(\frac{2\pi G}{M^2 P}\right)^{\frac{1}{3}} m \tag{2.4}$$

The full equation that takes into consideration the inclination, and the elliptical orbit and is not an approximation for $m << M$

$$v_{planet} = \left(\frac{2\pi G}{P}\right)^{\frac{1}{3}} \frac{m \sin i}{(m+M)^{\frac{2}{3}}} \frac{1}{\sqrt{1-e^2}} \tag{2.5}$$

where e is the eccentricity of the orbit and i the inclination (angle between normal to orbital plane and line of sight)

Jupiter - Io	β Pic b - exomoon
0.815 (m/s)	5.87 (m/s)

Table 2.3: The radial velocities of Jupiter caused by Io and β Pic b caused by a potential Earth-mass exomoon with 10 days period, calculated by using Equation (2.4).

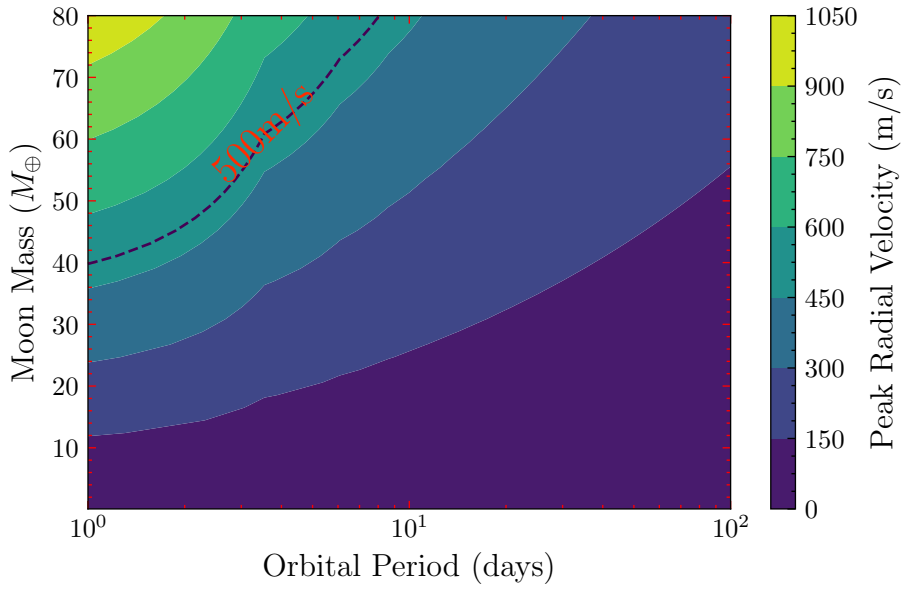

Figure 2.2: A contour plot showing the peak radial velocity for different masses and orbital periods of a potential exomoon around β Pic b. The mass is measured in Earth masses while the orbital period is measured in days. Radial velocity is in (m/s). Note that the x-axis showing the orbital period is in logarithmic scale. The dotted line is representing the isoline for 500 m/s.

For our case, all the approximations that went into Equation (2.4) are correct so we can use it to explain the amplitude in Figure 2.1. Jupiter has a smaller mass when compared to β Pic b which would lead to smaller radial velocities. However, this is not the case due to the different masses and periods of the moons. Io has a much smaller mass than the Earth, which is the mass of our potential exomoon, and also the period of Io is much smaller than the period of 10 days that we gave to the exomoon. The velocities that we derive by using Equation (2.4) are shown in Table 2.3

We see that they are consistent with what we get in Figure 2.1 as we would expect.

After that, we want to create a contour plot that will show the peak radial velocity for many different combinations of values of mass and orbital period. In Figure 2.2 we have the results for the planet β Pic b and the potential exomoons we might be able to observe around it.

The resolution of Figure 2.2 is 50×50 meaning that we created 2500 different simulations in order to get this result. The masses we selected were within the range of $[0, 80]M_{\oplus}$ which was split in 50, while the range of the orbital periods was $[0, 100]days$ which was also split in 50. We then took the radial velocities of each possible combination of the two in order to have an accurate contour plot with no inconsistencies.

The results as we would expect from both Equations (2.4) and (2.5) are showing a decline of the peak of the radial velocity as we go from bigger to smaller masses. The orbital period has the opposite effect, where we see that the increase of it leads to smaller peaks of the radial velocity.

A recent analysis of new observations (Rico Landman, private communication) indicates that soon we should be able to have the errors of the measurements of the radial velocity of β Pic b to be close to $500m/s$. This is the reason that we chose to indicate with a dotted isoline the level where peak radial velocity is at $500m/s$. This would mean that we should be able to observe any exomoon with a combination of mass and orbital period above this isoline but also even beyond that if we have enough observations.

Chapter 3

Cross correlation of convolved spectra

In this chapter, we will be working with two different model spectra of β Pic b.

The first high-resolution model spectrum of *beta* Pic b was provided by Dr Tomas Stolker. It was created as a best-fit from an atmospheric retrieval and calculated at a $\frac{\lambda}{\Delta\lambda} = 10^6$.

A second spectrum was provided by Dr Paul Mollière of the Max-Planck-Institut für Astronomie in Heidelberg, Germany. It is based on the best-fit model of GRAVITY Collaboration et al. (2020). The method used during this paper was to collect K-band spectro-interferometric data on β Pic b using the GRAVITY instrument in conjunction with the four 8.2 m telescopes of the Very Large Telescope Interferometer. They managed to obtain a high-precision astrometric location of the planet and medium resolution (R = 500) K-band spectra of the planet. Although the purpose was to measure the C/O ratio for the atmosphere of the planet, the spectrum can be reused for different purposes.

3.1 Methods

In order to be able to make use of these high-resolution spectra we first have to smooth them into a lower resolution. We can do that by rebinning the original spectra.

In order to do that we need to define our new wavelength bins and take the average flux of all the points that have a wavelength inside the lower and upper limits of the bin. All the bins have an equal size which depends on the number of bins we want to create.

The decision on how many bins to create is a compromise between wanting to keep as much information as possible and wanting to have a spectrum we can work with. We decided to go with 10^5 bins meaning our new low-resolution spectra will each consist of 10^5 data points.

After we are done with rebinning our spectra we need to convolve them using a normal distribution. In order to do that we first need to apply a window function in order not to have any boundary problems near the edges of our spectra.

We chose the cosine-tapered window, which is more commonly referred to as the Tukey window because it is simple to implement and fits our purposes. The formula of a Tukey window is

$$\begin{aligned} w(n) &= \frac{1}{2}(1 - \cos\frac{2\pi n}{aN}) \ , 0 \leq n \leq \frac{aN}{2} \\ w(n) &= 1 \qquad\qquad\qquad , \frac{aN}{2} \leq n \leq \frac{N}{2} \\ w(n-N) &= w(n) \qquad , \frac{N}{2} \leq n \leq N \end{aligned} \tag{3.1}$$

where N is the width of the function and a is the shape parameter of the Tukey window.

The function is symmetrical as indicated by the last part of the Equation (3.1) and has a value of 1 between $\frac{aN}{2}$ and $\frac{(2-a)N}{2}$ and decays using a cosine function towards the edges where the value goes to 0.

After applying this window on our rebinned spectra, we can convolve them with a normal distribution. By doing this the shared peaks count is generalized, which provides a more reliable indicator of spectral similarity. This makes the convolved spectrum more useful for further applications and analysis.

The process of convolution is done by shifting the array of the normal distribution along the x-axis and taking the sum of the product of the two arrays.

The formula for the convolution is:

$$(f * g)(x) = \int_0^x f(\kappa)g(x-\kappa)\,d\kappa \tag{3.2}$$

where f, g are the two initial functions and $(f * g)$ is the convolved function.

In our case of discrete convolution:

$$(f * g)[n] = \sum_0^M f[m]g[n-m] \tag{3.3}$$

where M is the length of our array.

To perform the calculations we use the SciPy library (Virtanen et al., 2020) which has the signal.convolve function using the "mode='Same' " in order to get the output at the same size as our initial spectrum (which is the rebinned version), centred with respect to the 'full' output which would have the size of the sum of the sizes of the two arrays.

The normal distribution array was produced with $mean = 0$ and $std = 1$ and was normalized so the sum of all the values is equal to 1. The length of the array after trying different sizes was decided to be 1080.

After getting the convolved spectra, we can now use them in order to simulate a Doppler shift caused by some radial velocity that the planet might have. In order to do that we implement the function pyasl.dopplerShift from the PyAstronomy library (Czesla et al., 2019).

We then attempt to calculate the velocity we used to Doppler shift the spectra, by cross-correlating its shifted spectrum with the original. For the cross-correlations, we use the signal.correlate function from the SciPy library. After getting the result of the cross-correlation and adjusting the x-axis to velocity units, the peak should be positioned at the velocity that is matching the one that was used for the Doppler shift.

The non-relativistic definition of the Doppler effect is

$$z = \frac{v}{c} \tag{3.4}$$

where v is the velocity of the object and z represents the shifting of the spectral lines

$$z = \frac{\Delta\lambda}{\lambda} \tag{3.5}$$

3.2 Results

In Figures 3.1 and 3.2 we can see the results of the processes of rebinning the original high-resolution spectra and the convolution of the rebinned spectra with a normal distribution.

The original spectra have 916,293 data points each, and as we can also see from Figures 3.1 and 3.2 they are not evenly spaced. By rebinning them we create an evenly spaced, across the wavelengths, data set, with 100 000 points which makes it easier to work with.

When we convolve the rebinned spectra with a normal distribution we are essentially smoothing all the edges. This creates spectra that don't have such a huge dispersion. This is clearly illustrated in both Figures 3.1 and 3.2 as we see the red line representing the convolved spectra is much more restrained when compared with both the original and the rebinned spectrum.

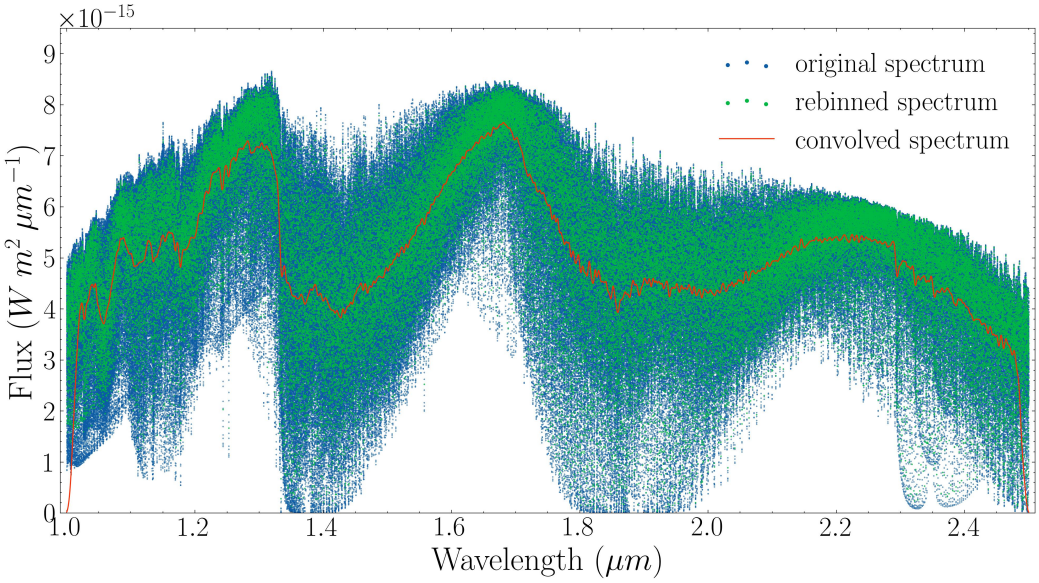

Figure 3.1: The high-resolution spectrum for β Pic b that was provided by Dr Tomas Stolker with the rebinned and convoluted versions. The wavelength is measured in μm while the flux is measured in $(W\,m^2\,\mu m^{-1})$

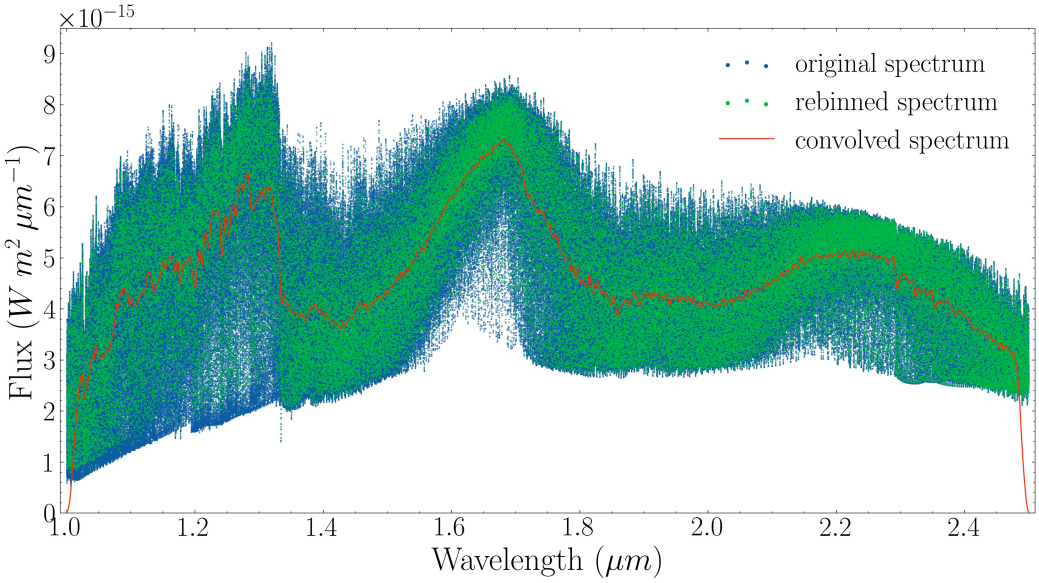

Figure 3.2: The high-resolution spectrum for β Pic b that was provided by Dr Paul Mollière (based on the best-fit model of GRAVITY Collaboration et al. (2020)) with the rebinned and convoluted versions. The wavelength is measured in μm while the flux is measured in $(W\,m^2\,\mu m^{-1})$

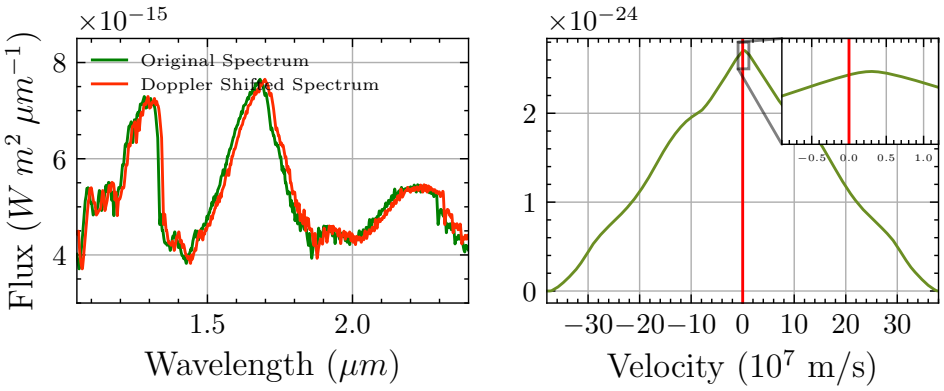

Figure 3.3: On the left panel: the convolved spectrum for β Pic b that was created from the high-resolution spectrum provided by Dr Tomas Stolker in green. The red line shows the shifted spectrum due to the Doppler effect with $v = 3000km/s$.
On the right panel: the result of the cross-correlation of the two spectra on the left. The vertical line represents the $v = 0$. On the small panel, there is the peak of the cross-correlation that is clearly at a non-zero velocity, close to $0.3 \times 10^7 m/s$.

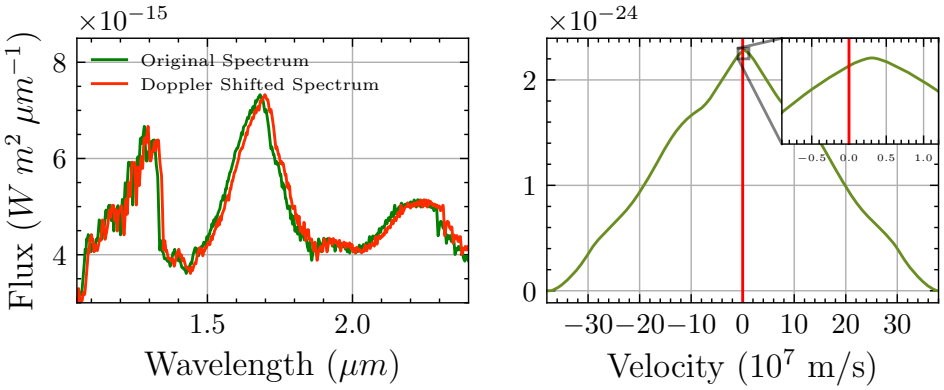

Figure 3.4: On the left panel: the convolved spectrum for β Pic b that was created from the high-resolution spectrum provided by Dr Paul Mollière (based on the best-fit model of GRAVITY Collaboration et al. (2020)) in green. The red line shows the shifted spectrum due to the Doppler effect with $v = 3000km/s$.
On the right panel: the result of the cross-correlation of the two spectra on the left. The vertical line represents the $v = 0$. On the small panel, there is the peak of the cross-correlation that is clearly at a non-zero velocity, close to $0.3 \times 10^7 m/s$.

In Figures 3.3 and 3.4 we can see the process of shifting the convolved spectrum using the Doppler shift and then calculating the velocity by cross-correlating the shifted with the original spectrum.

On the left, we find both the original and the shifted spectrum. We notice the small shifting that has occurred due to the Doppler effect. The velocity we used for the shifting was $v = 3000km/s = 3 \times 10^7 m/s$. This velocity is of course much higher than the typical radial velocities we expect an exomoon to be able to produce on β Pic b. It is however used as a starting point to test that we have a way of measuring radial velocities by using the cross-correlation technique.

The right part of Figures 3.3 and 3.4 is showing the result of the cross-correlation of the shifted spectrum with the original. If the two correlated spectra were identical we would expect to find the peak in the middle which is located at $v = 0$. We, however, notice a slim shift of the peak from the red line. The exact value of this dispersion is shown at Table 3.1

	Measured (m/s)	True (m/s)
1st Spectrum	$(3.009 \pm 0.004) \times 10^7$	3.000×10^7
2nd Spectrum	$(3.073 \pm 0.004) \times 10^7$	3.000×10^7

Table 3.1: The results of the cross-correlation for the two spectra with their Doppler-shifted counterparts. The second column gives us the position of the maximum correlation in m/s. In the last column, we have the true velocity which we used to shift each spectrum.

As we can see, we are able to accurately calculate the velocity we used to Doppler shift the spectra for both cases, with a small margin of error. This means that we have created an efficient way to measure radial velocities using cross-correlation. This method can also be used by adding noise to the data in order to simulate real data.

Chapter 4

Detecting simulated exomoons around β Pic b

In this chapter, we will simulate moons around β Pictoris b. We will then generate data in the form of radial velocity as a function of time that will be caused on the planet by the presence of the moon in orbit. On the data, noise will be added that is in agreement with the current and near-future measuring accuracy of radial velocities on the planet.

The next step is trying to see if we can realistically detect such an exomoon around the planet given the noisy data that we generated.

4.1 Methods

For the simulation of exomoons we will once again use the exoplanet module (Foreman-Mackey, Rodrigo Luger, et al., 2021b). When calling the module we need to specify the parameters of our simulation. We do that by defining the mass and radius of the central object to be equal to those of β Pic b. The inclination of the orbit is equal to $\frac{\pi}{2}$ creating an edge-on orbit, meaning the plane of the moon's orbit around the planet is parallel to the line of sight with the observer. Finally, all the orbits are defined with 0 eccentricities.

The mass and period of the orbiting object are defined differently every time we run the simulation in order to create many different scenarios and test the limits of the observable moons around the planet.

After creating the exomoon simulation, we want to generate the data of the radial velocities. We do that by creating 25 linearly spaced different data points across the span of 130 days. The reason behind this number is that it is a realistic attempt to find exomoons around β Pic b. The best period

for observations for β Pictoris b from the Paranal Observatory (VLT)[1] is between the months of September and December[2]. One possible proposal for observing the planet would consist of 25 one-hour-long exposures that can be accomplished during the second half of 2023. This gives us a bit more than three months. It is also worth noting that having the observations too far away from each other would make it more difficult to detect low-period exomoons which are our primary target since they produce greater radial velocities on the planet (see Figure 2.2).

The noise added to the generated data is based on the measuring accuracy of radial velocities on β Pic b. In Chapter 3 we discussed the measuring of radial velocities by cross-correlating the planet's spectrum. Based on the work of PhD candidate Rico Landman the current limit of observational error can be lowered to $500m/s$. This opens the doors for actually discovering exomoons around the planet or lowering the mass and period boundaries of potential existing exomoons in the event of a non-discovery. We are also testing on less noisy data ($250m/s$), in order to examine potential near-future discoveries and mass-period boundaries. We use a normal distribution to generate realistic noise around the true value of the simulated data.

After generating the noisy data we attempt to detect the moon based on the data with no prior knowledge of the orbit's parameters except some limits on the period. The limits on the period could not be avoided and are also realistic based on the range of periods we could observe by having one observation every 5.2 days and an observing span of 130 days. Also, periods greater than 30 days are not producing radial velocities on the host planet that could be detectable based on our discussion in Chapter 2 and particularly Figure 2.2.

In order to detect the exomoon we use the package PyMC3 (Salvatier et al., 2016b). Users of the Python application PyMC3 can fit Bayesian models using a variety of numerical techniques, most notably the Markov chain Monte Carlo approach (MCMC). The exoplanets module easily integrates with PyMC3 making it suitable for our usage.

We define the priors of our orbital parameters which are:

- period (range between 5 and 25 days)
- semi amplitude (normal distribution)
- eccentricity (range between 0 and 1)

[1]European Southern Observatory, n.d.(c).
[2]European Southern Observatory, n.d.(b).

and then define an agnostic orbit based on the exoplanet module. When we run our model, it optimizes for the different variables and then uses the MCMC method to create samples. The number of iterations to tune and the number of samples to draw was set to 1000, while the number of cores and chains was set to 2. If the model is successful in detecting the exomoon, the sampling will converge around the true period that we used to initially create the noisy data.

To visualise the results we also use the corner.py module (Foreman-Mackey, 2016) which creates corner plots of different variables. A corner plot is an illustration of different sample projections in high-dimensional spaces.

4.2 Results

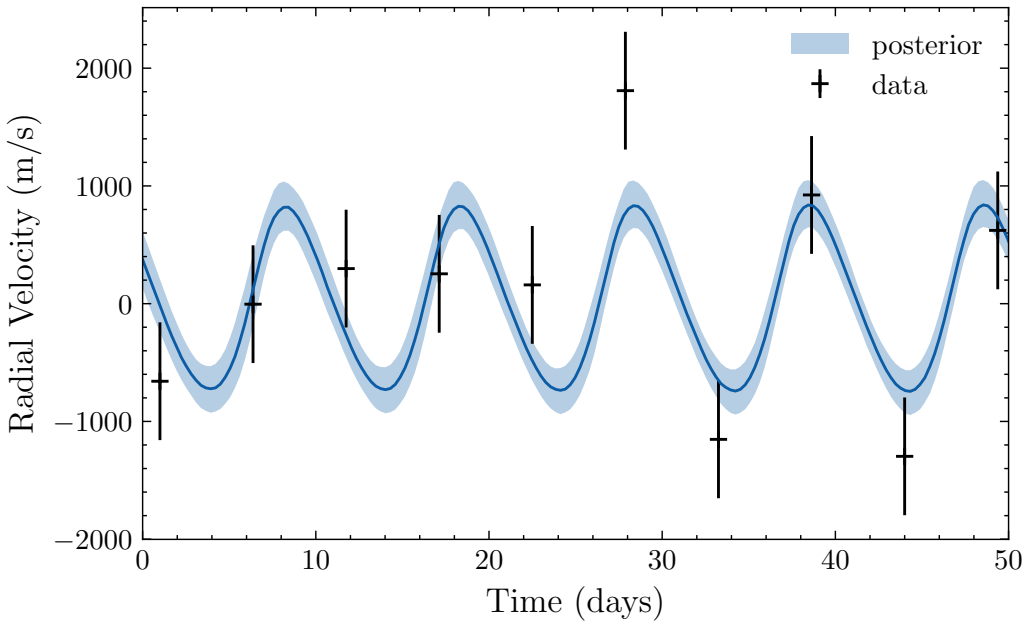

Figure 4.1: The radial velocity data generated from the exoplanet module for a moon of 80 Earth masses and a period of 10 days with added noise of $500m/s$. The blue line represents the posterior, after fitting the Bayesian model, with the 16th and 84th percentile.

We successfully performed many different simulations and exomoon detections. Each time we run the process of generating the radial velocity data, adding noise, fitting the Bayesian model and then plotting for visualisation.

In Figure 4.1 we can see the results of the Bayesian model fitting for the case of a potential exomoon of 80 Earth masses in an orbit with a period of 10 days. The noise added had an amplitude of $500m/s$. The chain used by the model accurately converged and the measured period was 10.09 days with a standard deviation of 0.08 days. This means that we can accurately detect an exomoon of this combination of mass and period if the accuracy of the measured radial velocities is $500m/s$.

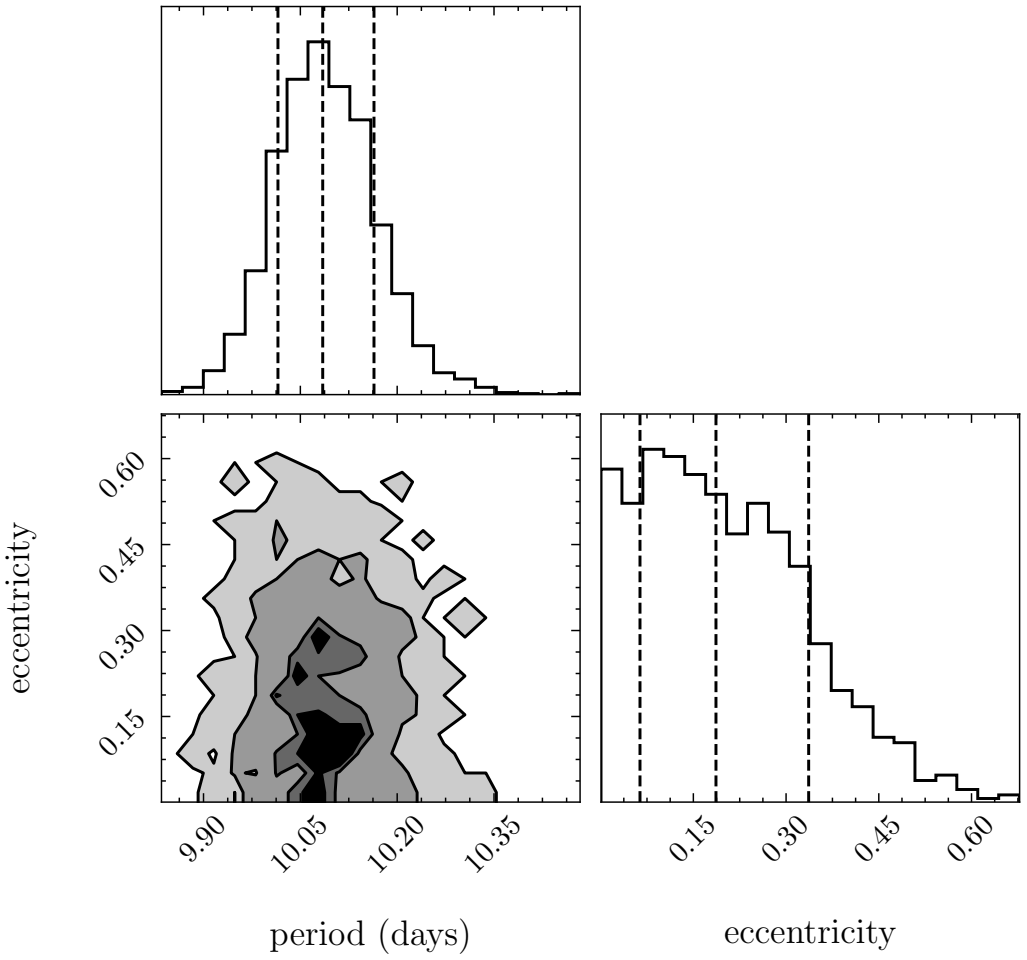

Figure 4.2: The corner plot of the orbital parameters of period and eccentricity after fitting a Bayesian model for a moon of 80 Earth masses and a period of 10 days with added noise of $500m/s$. The vertical lines show the 16th, 50th and 84th percentile of the posterior.

For the same simulation, we also have the corner plot as shown in Figure 4.2. We can see the full posterior of the orbital period and eccentricity

as well as the contour plot of both parameters. It is evident that there is no direct correlation between the two parameters and also the posterior of the orbital period has the shape of a normal distribution centred around the best-fitting value of 10.090 days. The posterior of eccentricity is less accurate but it also correctly favours lower values, as the original simulation was created with no eccentricity.

In our next example, we have a case where the noise used had an amplitude of $250m/s$. The exomoon that was simulated had a mass of 60 Earth masses and a period of 10 days.

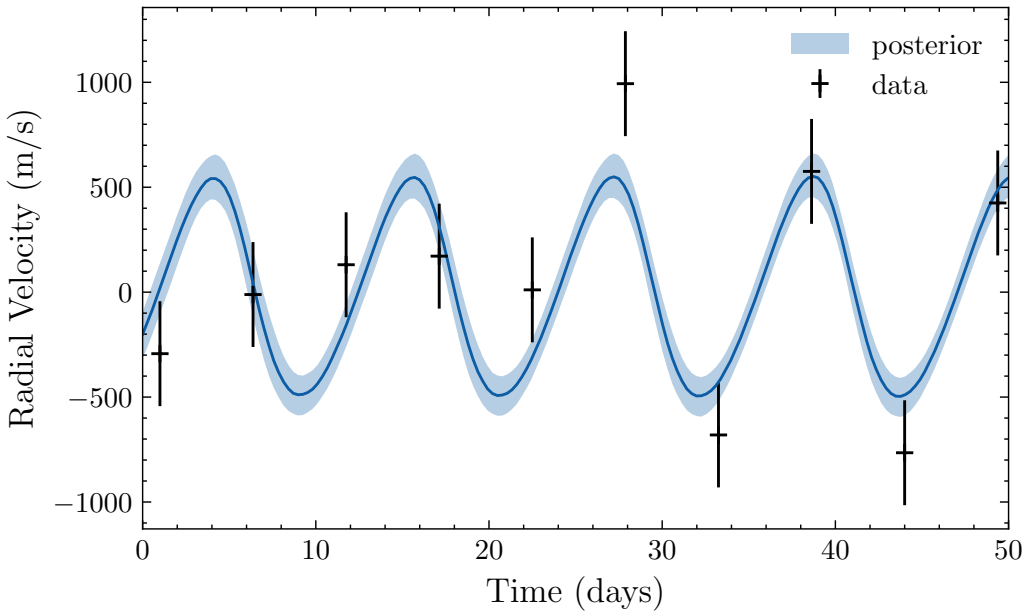

Figure 4.3: The radial velocity data generated from the exoplanet module for a moon of 60 Earth masses and a period of 10 days with added noise of $250m/s$. The blue line represents the posterior, after fitting the Bayesian model, with the 16th and 84th percentile.

In Figure 4.3 we can see the plot of the radial velocity as a function of time, including the noisy data generated from the simulation and the posterior of the Bayesian model that was fitted.

The corner plot for this fitting is shown at Figure 4.4. We can once again see that the posterior of the orbital period has the shape of a normal distribution centred around the best-fitting value of 11.53 days with a standard deviation of 0.08 days. This value is a bit off when compared to the actual orbital period of 10 days we used in the simulation it is however clear that the Bayesian model can detect the exomoon around the planet, although the

measurement of the period will not be accurate.

The posterior of eccentricity is accurate as it predicts low values with strong indications of a 0 value, considering there was no eccentricity when the initial simulation was built. On the contour plot, we can see the posterior of both the orbital period and eccentricity in the same plot.

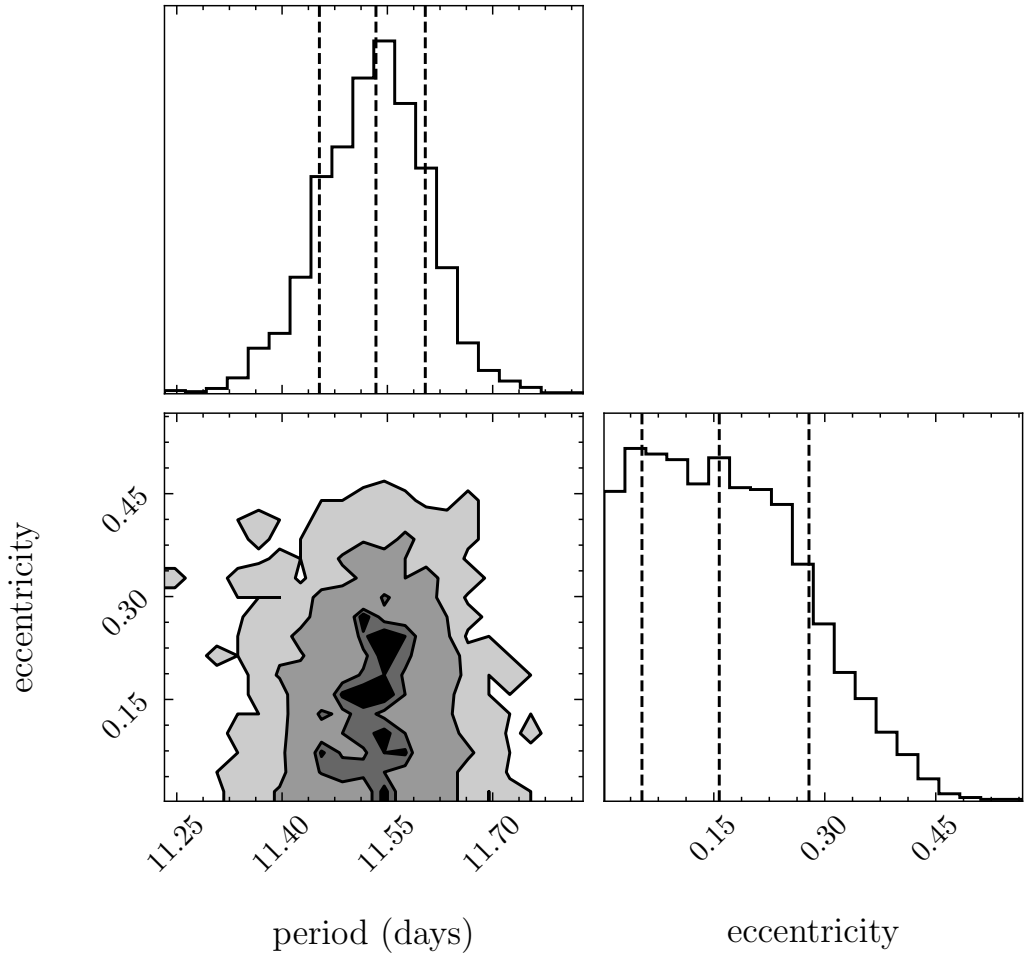

Figure 4.4: The corner plot of the orbital parameters of period and eccentricity after fitting a Bayesian model for a moon of 60 Earth masses and a period of 10 days with added noise of $250m/s$. The vertical lines show the 16th, 50th and 84th percentile of the posterior.

The process was repeated for 12 different cases. The simulation parameters as well as the measured orbital period with its standard deviation are shown in Table 4.1. In some of the cases, the chains used for the Bayesian model didn't converge, which becomes clear from the significant value of the

standard deviation compared with the actual measurement of the period. Those cases have their results underlined.

Each case falls into one of four different categories based on the orbital period of the moon (10 and 20 days) and also based on the amplitude of the noise that was added (250 and 500 m/s). For each category, we tested how low can the mass of a potential exomoon be, so that we are still able to accurately detect it.

Mass ($M_\oplus$)	Period (days)	Noise (m/s)	Pred. Period (days)	S.D. (days)
80	10	500	10.09	0.08
60	10	500	10.10	0.10
40	10	500	<u>15.19</u>	<u>17.6</u>
170	20	500	20.16	0.32
150	20	500	20.19	0.33
130	20	500	<u>31.92</u>	<u>49.5</u>
60	10	250	11.53	0.08
40	10	250	10.09	0.08
20	10	250	<u>12.92</u>	<u>14.0</u>
90	20	250	20.16	0.28
70	20	250	20.19	0.35
50	20	250	<u>32.49</u>	<u>39.1</u>

Table 4.1: The final results of all the simulations that were fitted with a Bayesian model. The first two rows show the mass (in Earth masses) and the period (in days) that was used during the simulation. The third row has the amplitude of the noise (in m/s) that was added to the radial velocity data. The final two rows are giving the measured period from the Bayesian model and the standard deviation (S.D.) in days. The cases where the chains used by the model didn't converge are shown by underlying the period results.

In Appendix A we can find the radial velocity versus time plots as well as the corner plots for all the 10 different cases that were not shown in this chapter.

In Chapter 6 we can also find a table that is summarising the result of the experiment we ran in this chapter. Table 6.1 is showing the lowest mass threshold below which we were not able to accurately detect the exomoon for each of the four categories we discussed.

Chapter 5

Explaining the RV data with the Rossiter-McLaughlin effect

In this chapter, we will work with real data for the planet β Pictoris b. The work for extracting the radial velocity data from the high-resolution spectra was accomplished by Rico Landman.

The data were obtained from CRIRES+ observations, a high-resolution spectrograph on the VLT[1]. The observations for β Pic b were done both on November 11 and 13, 2022. The duration of each observational run was 1 hour. The data were reduced using pycrires (Stolker, 2021) and the official esorex pipeline. The approach from Ruffio et al. (2019) was then used to estimate the radial velocity of the planet.

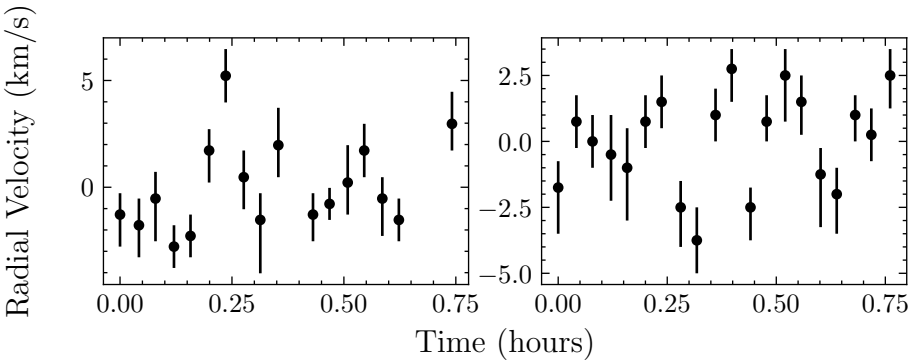

Figure 5.1: The radial velocity data for β Pictoris b that were provided by Rico Landman. The two panels contain the two separate observational runs on November 11 (left) and November 13 (right) of 2022.

[1]European Southern Observatory, n.d.(a).

The result of this process is shown in Figure 5.1. The data consist of two observational runs. For the first one, we get 17 data points (left panel of Figure 5.1). For the second observational run (right panel), there are 20 data points.

We will analyze this data in a search for an explanation for the very short time fluctuations that were observed. One plausible explanation could be the existence of various spots on the surface of β Pic b. In this chapter, we will explore if we can indeed match the data with a certain spot pattern.

The existence of spots on the surface of any astronomical object will create a radial-velocity variation happening over the Doppler reflex motion, similar to the one created by another object orbiting around our main astronomical object (Triaud, 2018). This is known as the Rossiter–McLaughlin effect and is mainly used in observations of exoplanets around stars. In our case, it can be used to explain the peculiar radial velocity data of the planet β Pic b, by assuming the existence of various spots that could match the observed data.

5.1 Methods

In order to simulate the spots on the surface of the planet we will use the starry code package (Rodrigo Luger, Foreman-Mackey, Hedges, and Hogg, 2021; Rodrigo Luger, Foreman-Mackey, and Hedges, 2021a; Rodrigo Luger, Foreman-Mackey, and Hedges, 2021b; Rodrigo Luger, Bedell, et al., 2019; Rodrigo Luger, Agol, et al., 2019).

An array of spherical harmonic coefficients serves as the description of surface mapping in starry. Spherical harmonics constitute a complete basis on the surface of the sphere, just like polynomials do on the real number line. If one expands to a high enough degree, any surface map can be described as a linear combination of spherical harmonics.

We implement the starry package by declaring the parameters that correspond to the planet we want to simulate, which are the mass and radius. In our case, we want to simulate the planet β Pic b, for which we have the radial velocity data. After doing that we can create spots on the surface of the planet by declaring the size of the spot and its location (latitude and longitude), as well as the equatorial velocity of the planet's surface. We are able to create multiple spots and after doing so, take the radial velocity data.

In Figure 5.2 we can see how the spots are being created using this package. For this particular example, we created 6 spots across the equator of the planet.

The limitations of the starry package don't allow us to declare as many spots as we want. When setting up the simulations we could not retrieve any

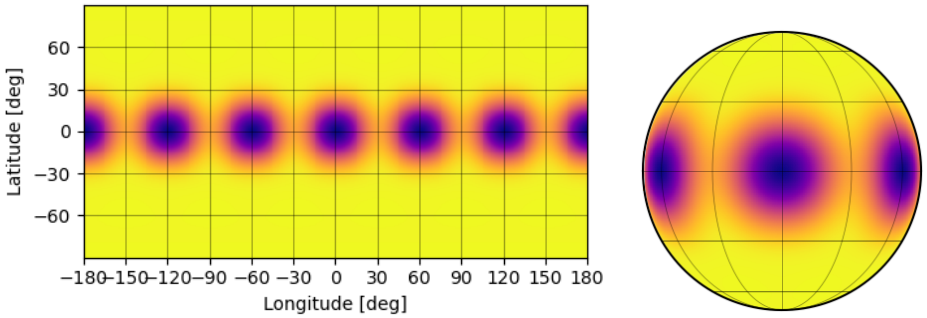

Figure 5.2: Spot creation using the starry package. For this figure, we created 6 spots with 0 latitude and different longitudes. On the left, we see the equirectangular view of the map while on the right panel we find the spherical view of the planet with the spots.

meaningful radial velocity data for more than 11 spots. One other limiting factor is the minimum size of these spots. The starry package documentation makes it clear that the user can only create spots with a radius equal to or greater than 15 degrees.

While these limitations don't allow us to explore the whole range of possible spot arrangements on the surface of the planets we can still use the library to get as much data as we can and then extrapolate to find a plausible number of spots that could match the data we have.

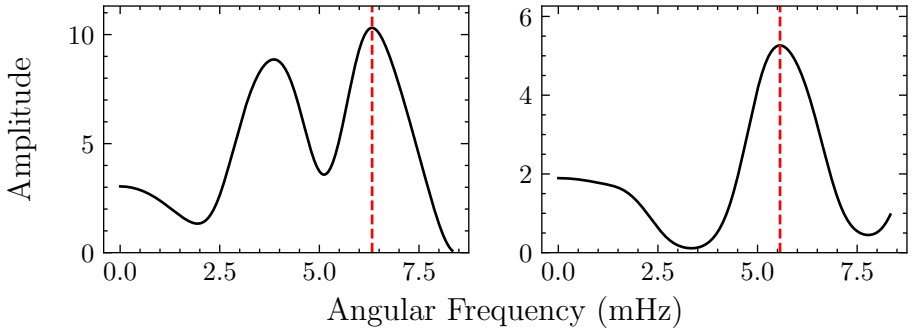

Figure 5.3: The Fourier Transformation of the radial velocity time-series shown in Figure 5.1. On the left panel, we have the first observational run, while the second one is on the right panel.

5.2 Results

Before simulating the spots on the surface of the planet we want to analyze the radial velocity data. In Figure 5.3 we can find the Fourier Transformation of the time series shown in Figure 5.1.

We can see that both observational runs have a similar frequency peak at around 5.5 mHz.

We use the peak frequency of each one, in order to fit a sinusoidal function on the time series. The fitting function uses the formula:

$$f(x) = f(t) = a \times t + b \sin(c \times t + d) \tag{5.1}$$

where a, b, c, d are the 4 parameters of our function.

We are mainly interested in parameters b, c which represent the amplitude and angular frequency of our signal.

Before fitting the function we transform the time series to be centred around 0, by subtracting the average radial velocity of each observational run respectively. We also make the time series symmetrical around t=0. These transformations will make it easier to fit our model and will not affect the final results of the fitting.

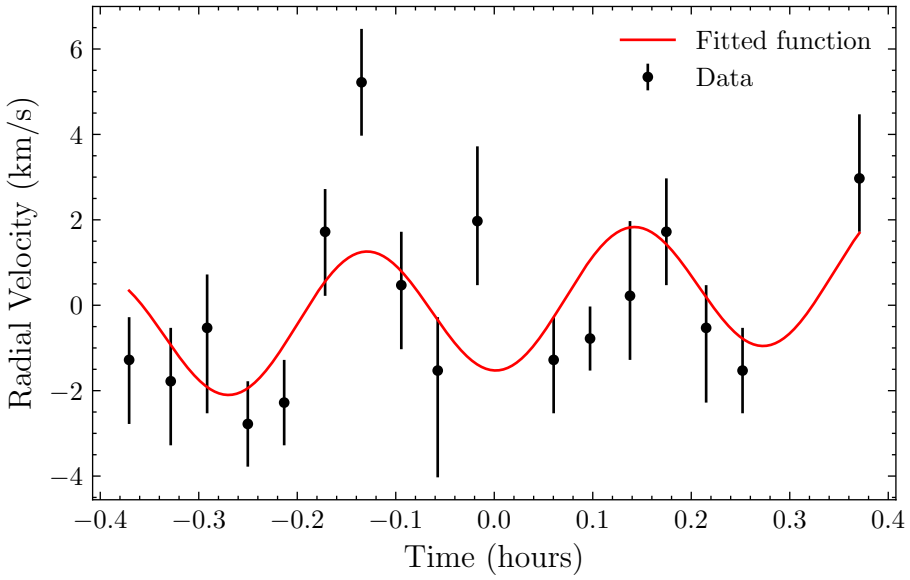

Figure 5.4: The radial velocity data for the first observational run with the fitted function. The data were transformed by subtracting the average radial velocity and were also made to be symmetrical around $t = 0$. The model used for the fitting can be found in Equation (5.1).

The results for both observational runs are shown in Figures 5.4 and 5.5. We see that despite some inaccuracies the main shape of the data can be explained with our simple model.

The values of the main parameters of interest are shown in Table 5.1. As we already discussed parameters b, c represent the amplitude and frequency of our signal, so we extract the values and errors after fitting our model in both observational runs.

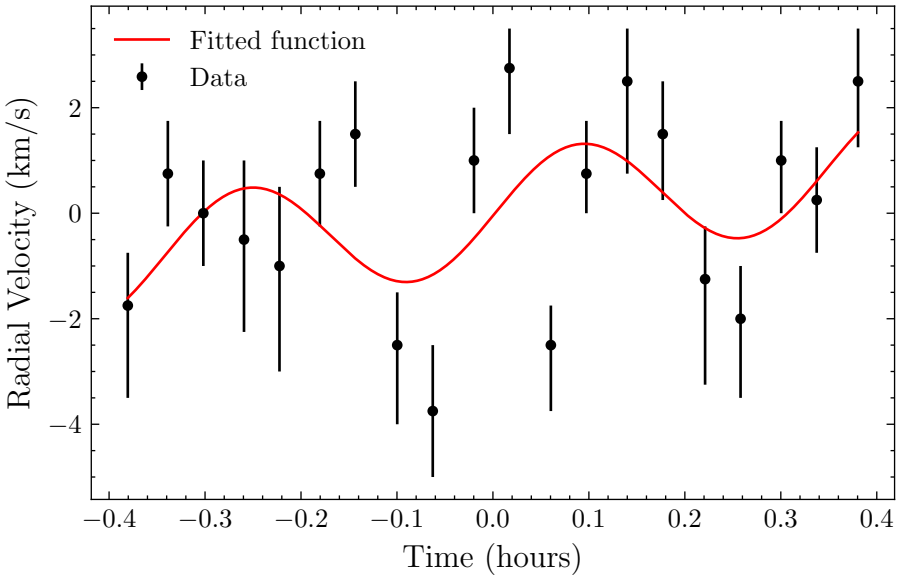

Figure 5.5: The radial velocity data for the second observational run with the fitted function. The data were transformed by subtracting the average radial velocity and were also made to be symmetrical around $t = 0$. The model used for the fitting can be found in Equation (5.1).

The angular frequencies for the two observations have a plausible overlap on the error bars. This is a great indication of some mechanism that is responsible for producing both main frequencies. Due to the rotation of β Pic b, different surface features can appear and affect the radial velocities that we observe, which would explain the minor difference.

The difference in the signal amplitude is even smaller and the overlap of the error bars is even more clear. That is another indicator of one mechanism responsible for both observed signals, with minor changes.

	Ang. Frequency (mHz)	Period (hours)	Amplitude (m/s)
1st Observation	6.43 ± 0.61	0.271 ± 0.026	1.53 ± 0.37
2nd Observation	5.06 ± 0.74	0.345 ± 0.05	1.09 ± 0.33

Table 5.1: The values of the fitting parameters that correspond to the angular frequency and amplitude of the signal after fitting our model (Equation (5.1)) for both observational runs.

After analyzing the radial velocity signals for the two observational runs we can attempt to explain them using the starry package to create spots on the surface of β Pic b.

We simulate multiple spots, all on the same latitude each time. Keeping the number of spots fixed we change the latitude to measure the effects of such change. We then increase the number of spots and repeat the process.

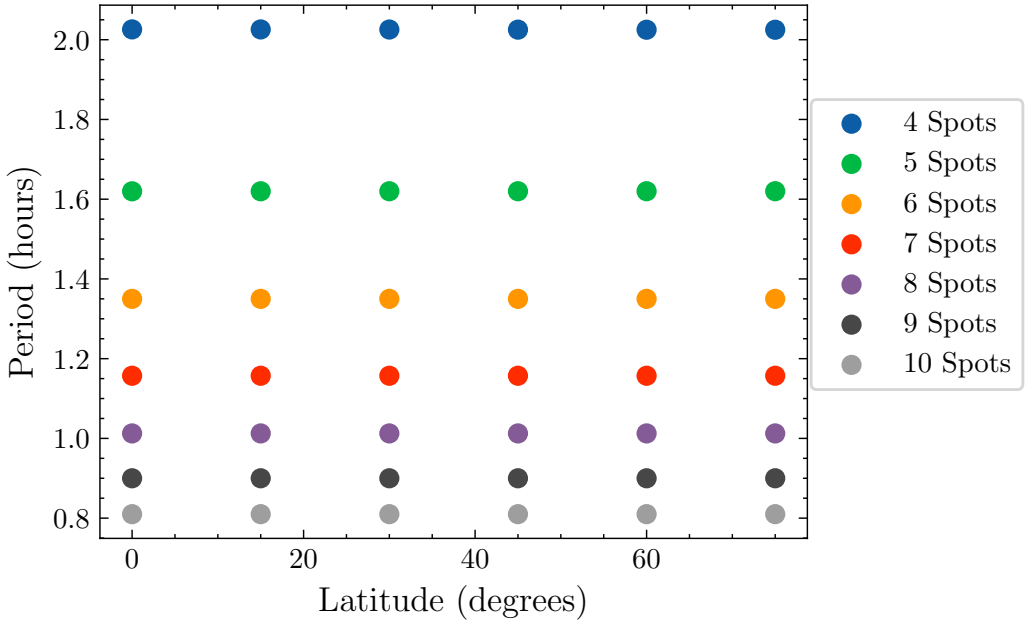

Figure 5.6: The period of the radial velocity signal as a function of the latitude. The different colours represent a different number of spots that were simulated. There is no significant difference in the period as the latitude changes, while the number of spots is the only factor that affects the periodicity.

After simulating many different scenarios we extract the period and am-

plitude of each signal. In Figure 5.6 we can see how the number of spots on the planet's surface as well as the latitude that these spots can be found affects the period of the radial velocity signal.

It is clear that latitude plays no role in the frequency of the signal. The only factor that affects this periodicity is the number of spots on the planet.

We can use this fact to calculate the number of spots that can explain the measured frequencies in Table 5.1, by extrapolating from our simulations.

In Figure 5.7 we can see the period of the signal as a function of the number of spots. We use this data in order to fit a one-parameter inverse function

$$f(x) = a\frac{1}{x} \tag{5.2}$$

The function fits our data perfectly with a value of $a = 8.1004 \pm 0.0002$. This result is also shown in Figure 5.7 with the red line.

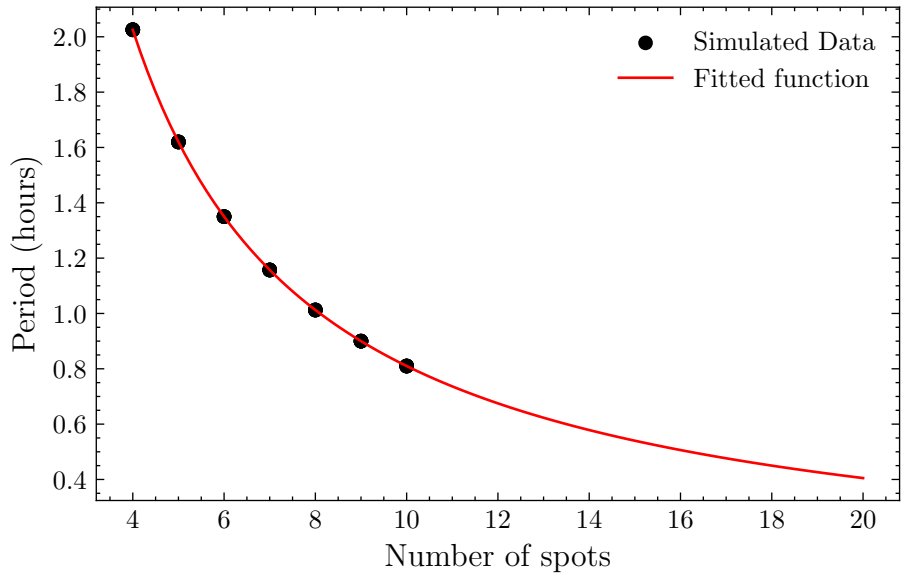

Figure 5.7: The period of the radial velocity signal as a function of the number of spots on the atmosphere of β Pictoris b. The red line represents the fitted function, which uses the formula in Equation (5.2).

We can use the function we fitted on the simulated data to extrapolate to the measured frequencies in Table 5.1. By doing so, we calculate the number of spots on the surface of β Pic b that can in theory explain the observed fluctuations of the radial velocities we observed.

In Table 5.2 we find the results from the extrapolation. We see that the number of spots required to explain the two signals could potentially be the

	Measured Period (hours)	Number of Spots
1st Observation	0.271 ± 0.025	27 - 33
2nd Observation	0.345 ± 0.05	21 - 27

Table 5.2: The number of spots that could explain the observed period of the radial velocity signal in the two observational runs.

same as it is within the margin of error in the radial velocity measurements. Also, this number is well beyond what could be simulated using our basic model. It is however plausible that the existence of spots on the atmosphere of β Pic b could explain the signals we are receiving and our work shows that the scale of such phenomena is of similar magnitude and can produce frequencies similar to the ones we are observing. Because the latitude of the spots plays no role in the period of the change in radial velocity there is no reason that all these spots have to be on the same parallel.

Trying to explain the amplitude of the two signals is an even harder task due to the limitations that come from the starry package.

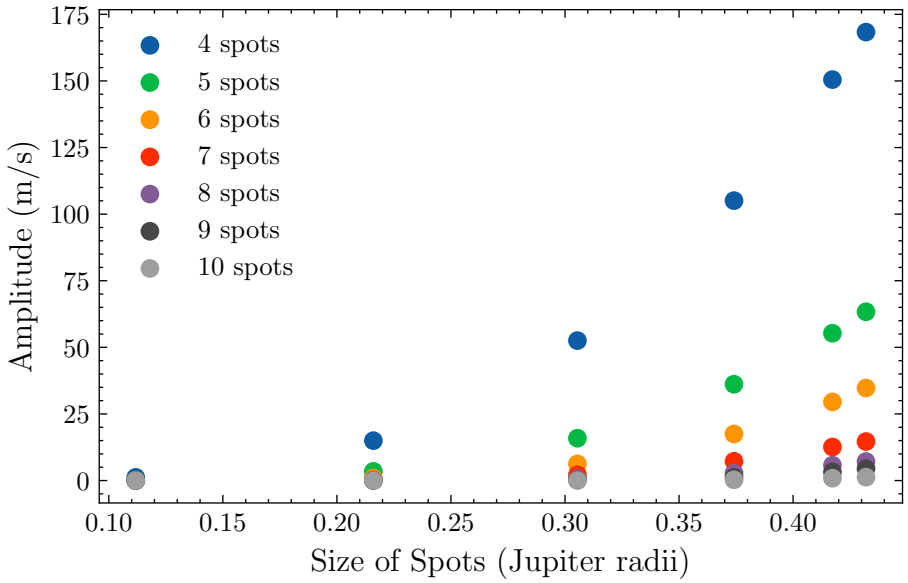

Figure 5.8: Radial velocity amplitudes as a function of the size of the spots. The colours indicate the number of spots that were used in the simulation.

In Figure 5.8 we see that the radial velocity amplitude increases rapidly as the size of the spots increases. However, as is also shown in the same

figure, the number of spots also plays a huge role in the amplitude in the opposite direction. As the number of spots increases, the signal amplitude decreases.

There is no way we can extrapolate in both directions (number and size of spots) in order to explain the amplitudes we observed during the two runs. We however note that it is not unreasonable to believe that such a combination can exist.

Although we were not able to fully explain the radial velocity data by assuming the existence of spots on the atmosphere of β Pic b due to our limitations, we got many indications that the scale of such phenomena can possibly factor in to produce the received signals. Other atmospheric phenomena, such as zones with different rotational periods, can also be explored and possibly play a role.

Chapter 6

Conclusions

One thing that was very clear from the beginning was that searching for exomoons by radial velocity is a very challenging task that tests the limits of our current technology and detection techniques. We wanted to navigate through all that and find potential planets where we could potentially achieve that in the near future. Our work greatly focused on the planet β Pictoris b. The reason is that it is a great target for collecting radial velocity data, because of its location and the almost perfect edge-on orbital orientation with respect to our planet.

In this current work, we started by laying out some useful and more general information on exoplanets in general while focusing more on exomoons. Our introduction (Chapter 1) ended with more specific information on β Pictoris b, which was analysed throughout this work.

After that, we probed into the effects moons have on the radial velocity of their host planets. In Chapter 2 we compared potential exomoons around β Pictoris b and Io, the moon of Jupiter. One of the most interesting results came in Figure 2.2 where we plotted the radial velocity on the planet as a function of both the mass of the moon and its orbital period.

We also wanted to test the way we measure radial velocities, using simulated spectra for β Pictoris b. Each spectrum was transformed and convolved before applying a Doppler shift. We then used cross-correlation to successfully extract the velocity that was used for the shifting. The details of this work are shown in Chapter 3.

In Chapter 4 we simulated the detection of an exomoon around β Pictoris b from the beginning. At first, we created the simulated radial velocity data for many different combinations of mass and period of the potential exomoon. We then added noise to the data in order to test if a detection would be possible under those conditions. After that, we used a full Bayesian Model fit in order to measure the period and eccentricity of the simulated moon's

orbit.

The information we got from this experiment was crucial. We were able to see how much mass an exomoon should have in order for it to be detected. The answer greatly depends on the period of the moon because the further away it is, the less impact it has on the radial velocity of the planet.

	Period	
Noise	10 days	20 days
$250\,m/s$	$> 20M_{\oplus}$	$> 60M_{\oplus}$
$500\,m/s$	$> 40M_{\oplus}$	$> 130M_{\oplus}$

Table 6.1: The four different categories that we used to simulate the radial velocity data of the exomoons. For each category, we note the threshold for the exomoon to be detectable using our Bayesian model.

In Table 6.1 we find the thresholds for the mass of the exomoons. For each category (based on the noise and period), detection of potential exomoons with a mass lower than the one given in this table is not possible with our model. This consists of the lower limits, meaning that the chains used by our Bayesian Model did not converge for the given masses. They did however converge for every mass above this threshold.

One of the issues we faced during this work was the lack of real radial velocity data on β Pictoris b that would be applicable to use for exomoon detection. In Chapter 5 we worked with some preliminary data that came from Rico Landman, consisting of two observational runs. The task was to determine if the strange behaviour that was observed could be explained by the potential existence of spots on the atmosphere of the planet, using the Rossiter-McLaughlin effect. If this is successful it could vastly increase the measuring accuracy of radial velocities for this planet, and also open the door for similar work on other planets as well.

In our work, we showed that it is possible that spots can cause radial velocity signals that can have the same frequency as the main frequency we observed on the data we acquired. Explaining the amplitudes was not possible due to the limitations of the packages we were using. We however note that it is not unreasonable as we have shown the rapid growth of the radial velocity signal amplitude with respect to the size of the spots.

To summarise in our current work we explored the potential of exomoon detections while focusing more on the planet β Pictoris b, a perfect candidate due to its orbit characteristics and observability. We tested our current and

future limitations on the mass we would expect such detection to have. We also collaborated with other scientists to try to explain the behaviour of radial velocity signals, by simulating spots on the planet.

Appendix A

Bayesian Model Fitting Plots

In this appendix, we include all the plots for the Bayesian model fitting that we didn't show in Chapter 4. Each page below has two plots for each of the 10 cases.

First is the radial velocity as a function of the time plot. The radial velocity data from the exoplanet module, with additional noise, are included in this plot. The posterior of the Bayesian model fitted is shown by the blue line with the 16th and 84th percentiles. The second plot that is included for each case is the corner plot of the orbital parameters of period and eccentricity after fitting the Bayesian model. The vertical lines show the 16th, 50th and 84th percentile of the posterior.

Each case is labelled with the mass and orbital period of the simulation as well as the amplitude of the noise that was used.

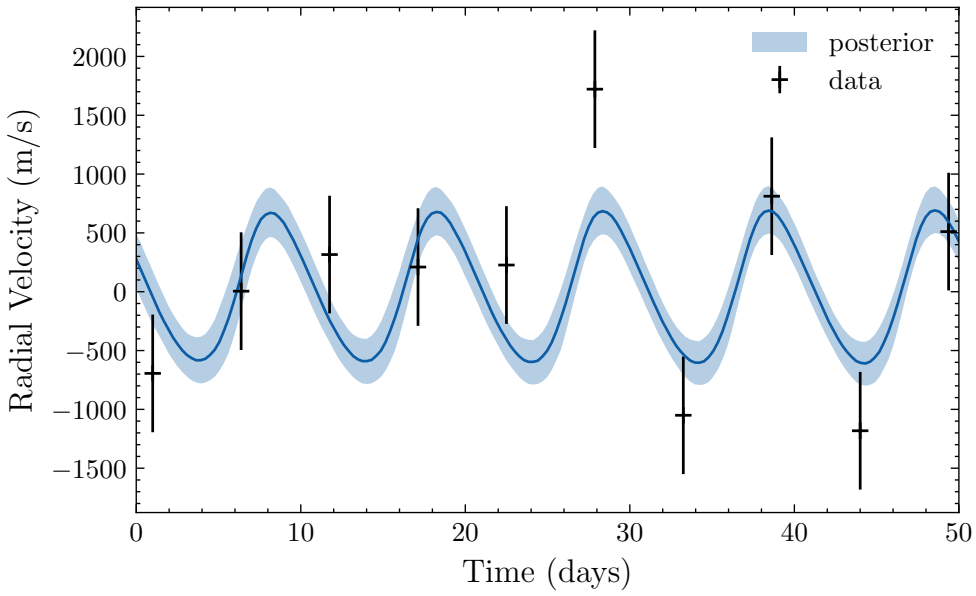

Figure A.1: Period: 10 days, Moon Mass: 60 $M_{\oplus}$, Noise= 500 m/s

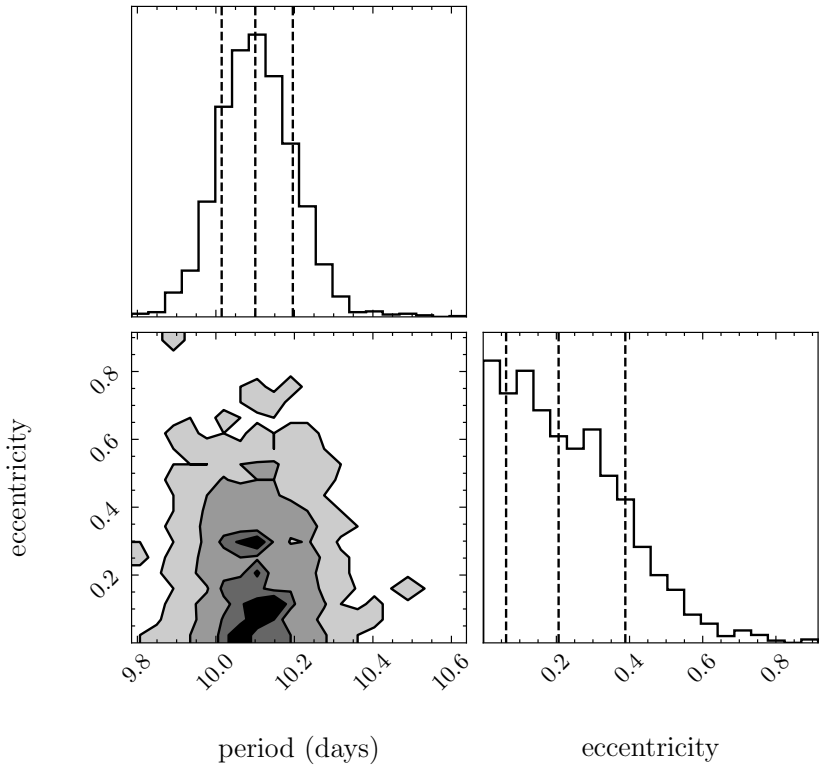

Figure A.2: Period: 10 days, Moon Mass: 60 $M_{\oplus}$, Noise= 500 m/s

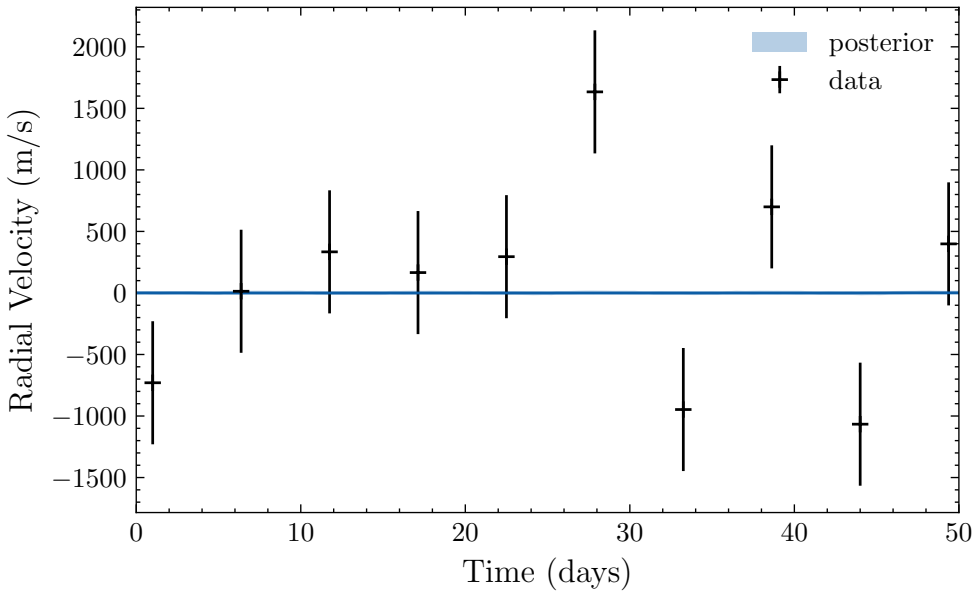

Figure A.3: Period: 10 days, Moon Mass: 40 $M_{\oplus}$, Noise= 500 m/s

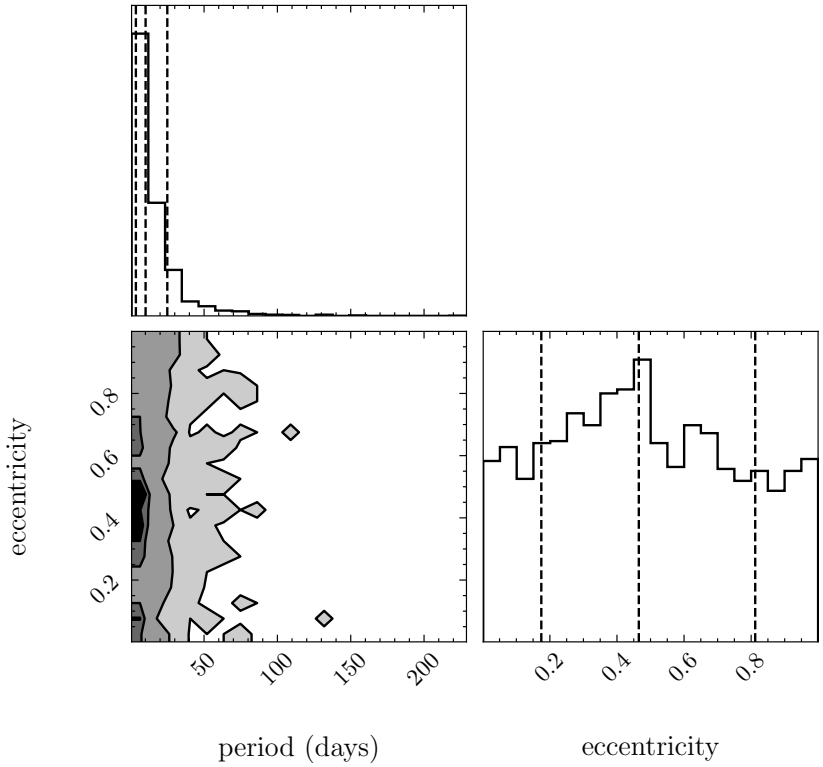

Figure A.4: Period: 10 days, Moon Mass: 40 $M_{\oplus}$, Noise= 500 m/s

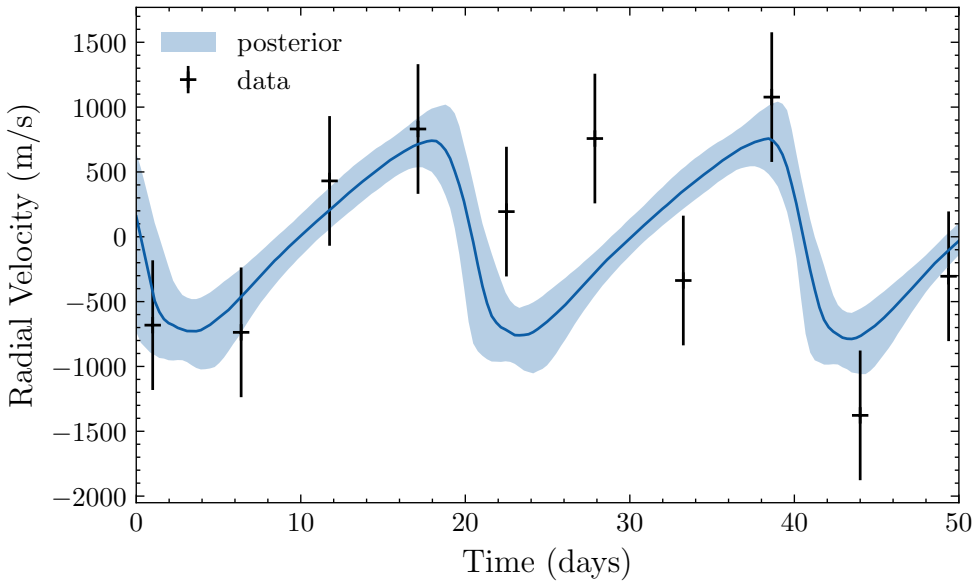

Figure A.5: Period: 20 days, Moon Mass: 170 $M_{\oplus}$, Noise= 500 m/s

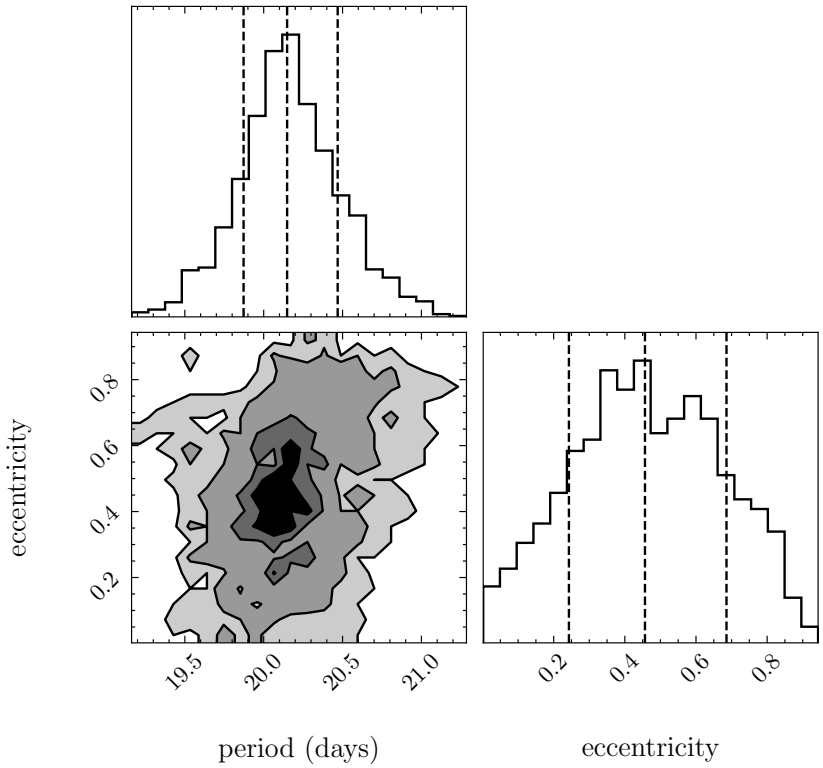

Figure A.6: Period: 20 days, Moon Mass: 170 $M_{\oplus}$, Noise= 500 m/s

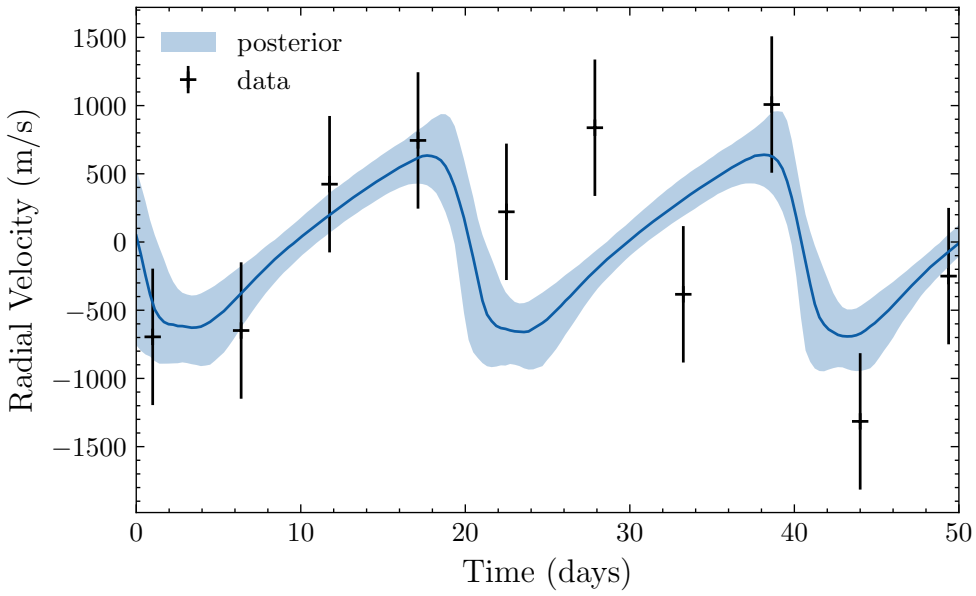

Figure A.7: Period: 20 days, Moon Mass: 150 $M_{\oplus}$, Noise= 500 m/s

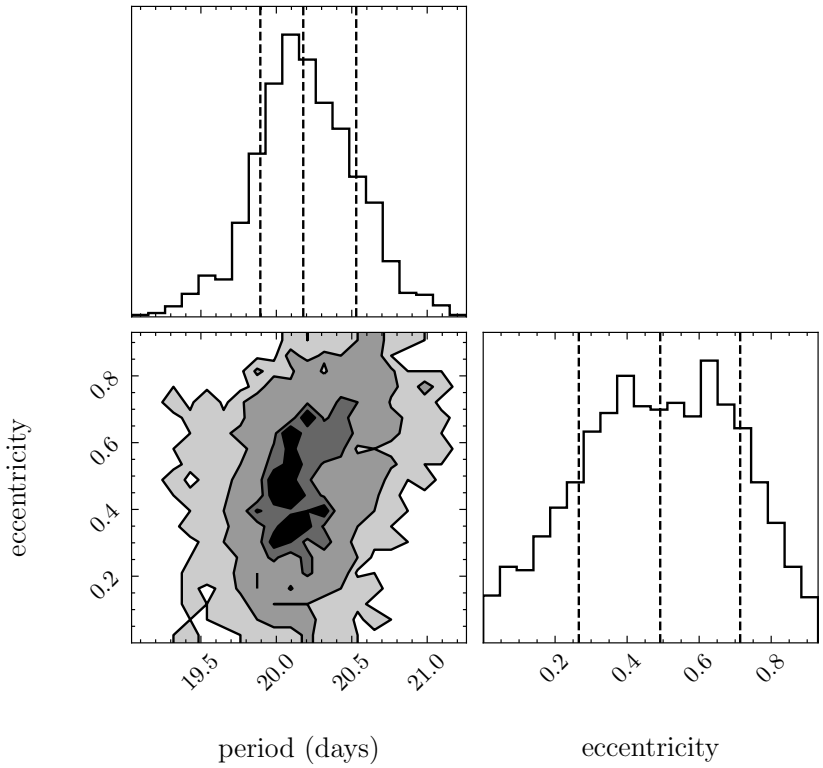

Figure A.8: Period: 20 days, Moon Mass: 150 $M_{\oplus}$, Noise= 500 m/s

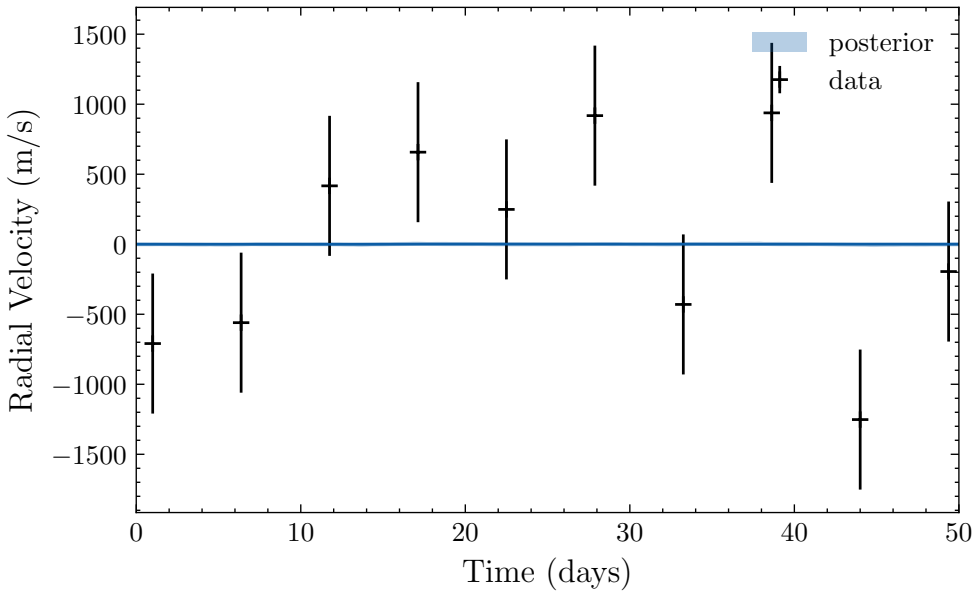

Figure A.9: Period: 20 days, Moon Mass: 130 $M_{\oplus}$, Noise= 500 m/s

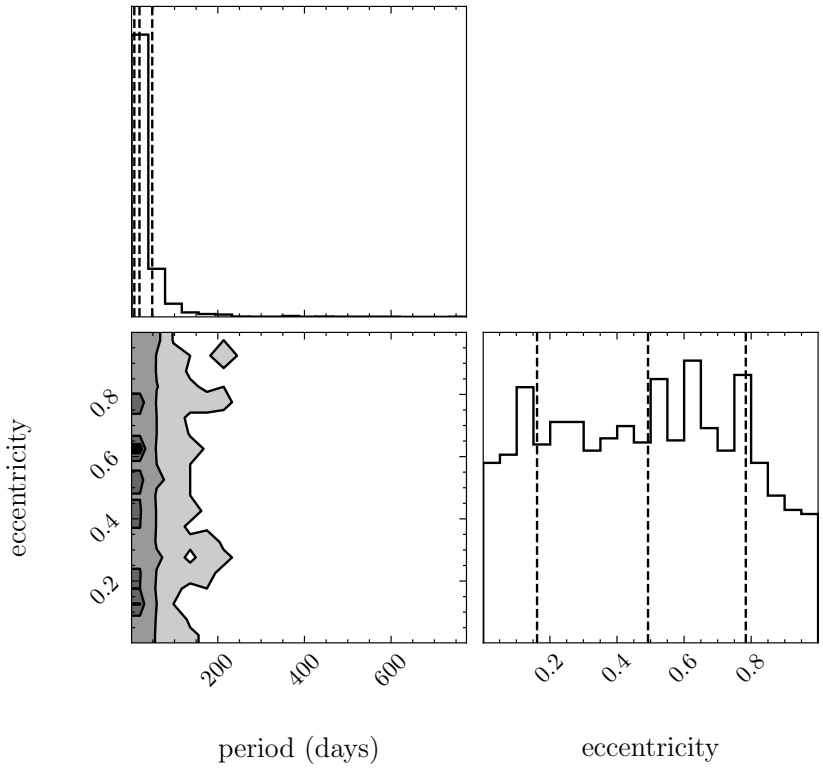

Figure A.10: Period: 20 days, Moon Mass: 130 $M_{\oplus}$, Noise= 500 m/s

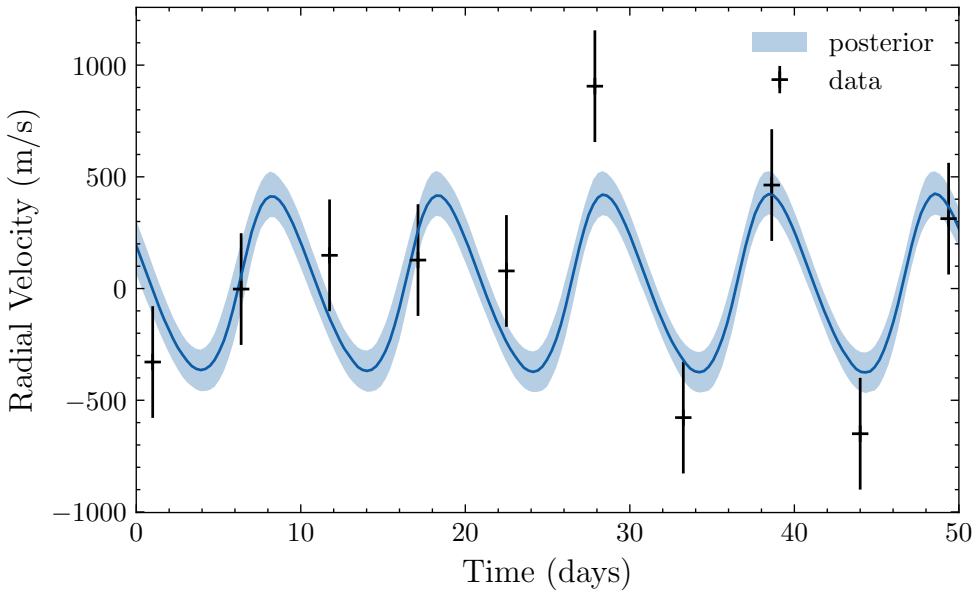

Figure A.11: Period: 10 days, Moon Mass: 40 $M_{\oplus}$, Noise= 250 m/s

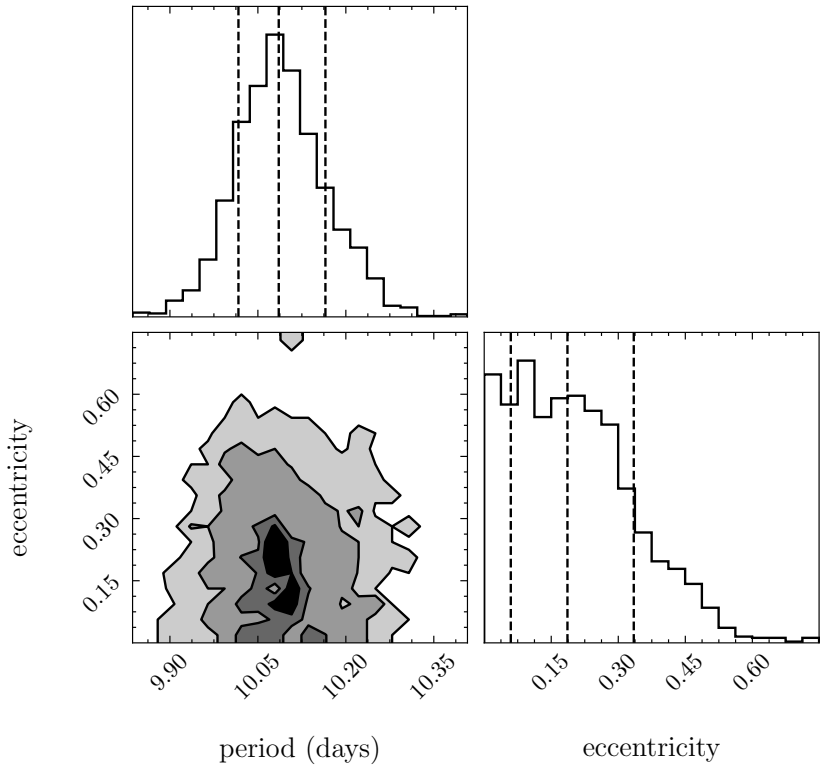

Figure A.12: Period: 10 days, Moon Mass: 40 $M_{\oplus}$, Noise= 250 m/s

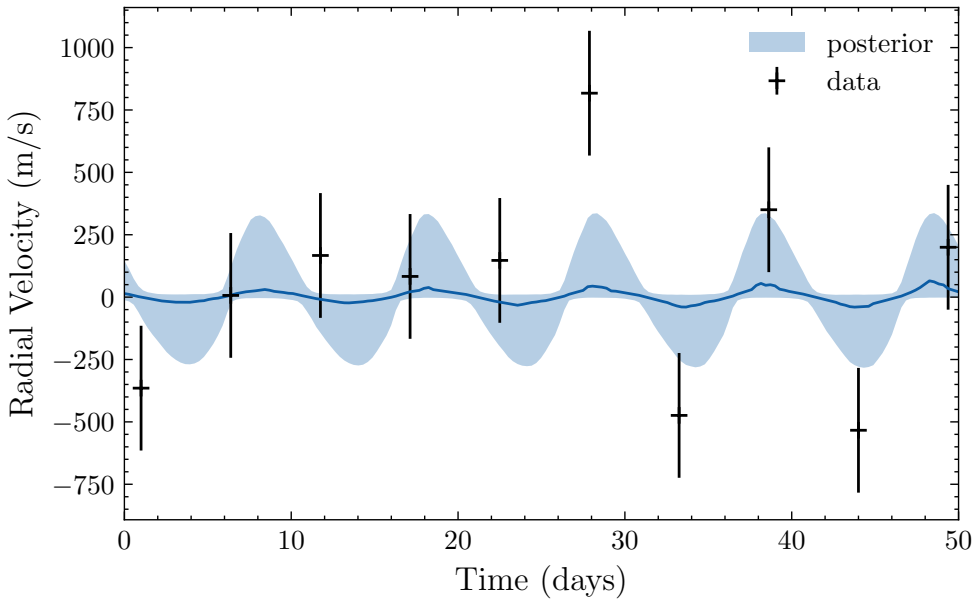

Figure A.13: Period: 10 days, Moon Mass: 20 $M_{\oplus}$, Noise= 250 m/s

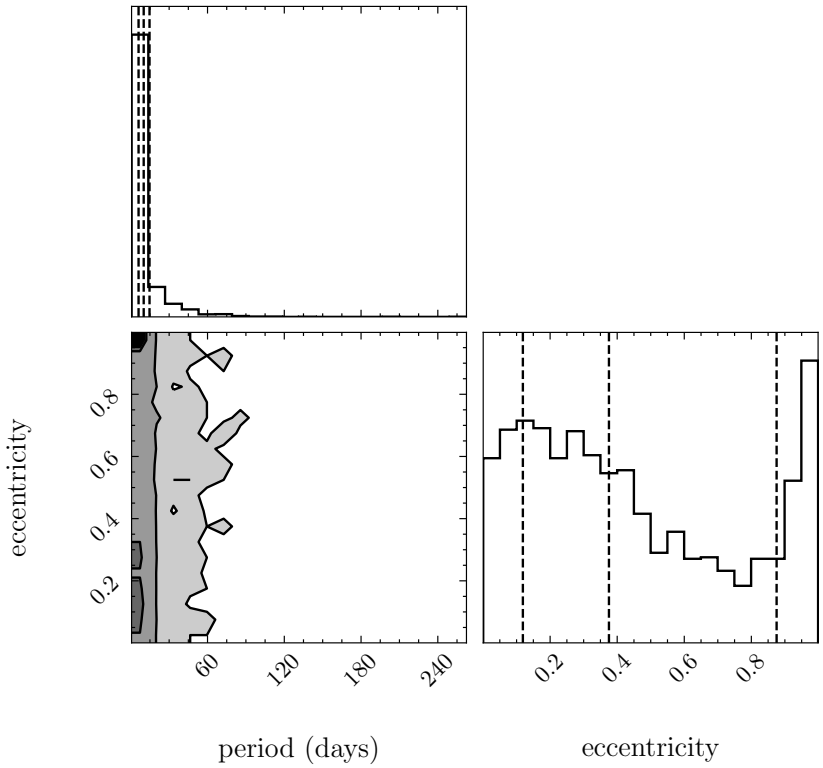

Figure A.14: Period: 10 days, Moon Mass: 20 $M_{\oplus}$, Noise= 250 m/s

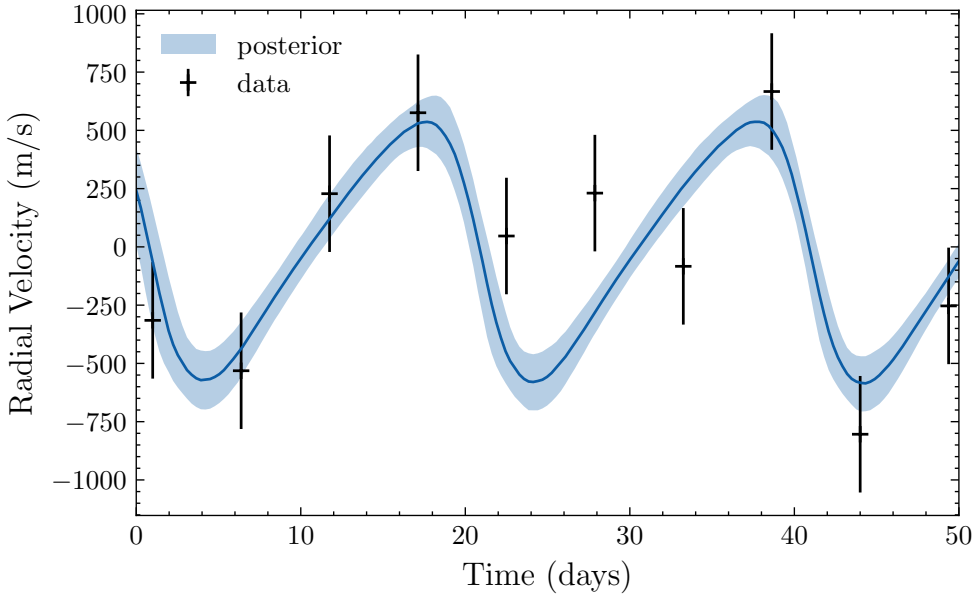

Figure A.15: Period: 20 days, Moon Mass: 120 $M_{\oplus}$, Noise= 250 m/s

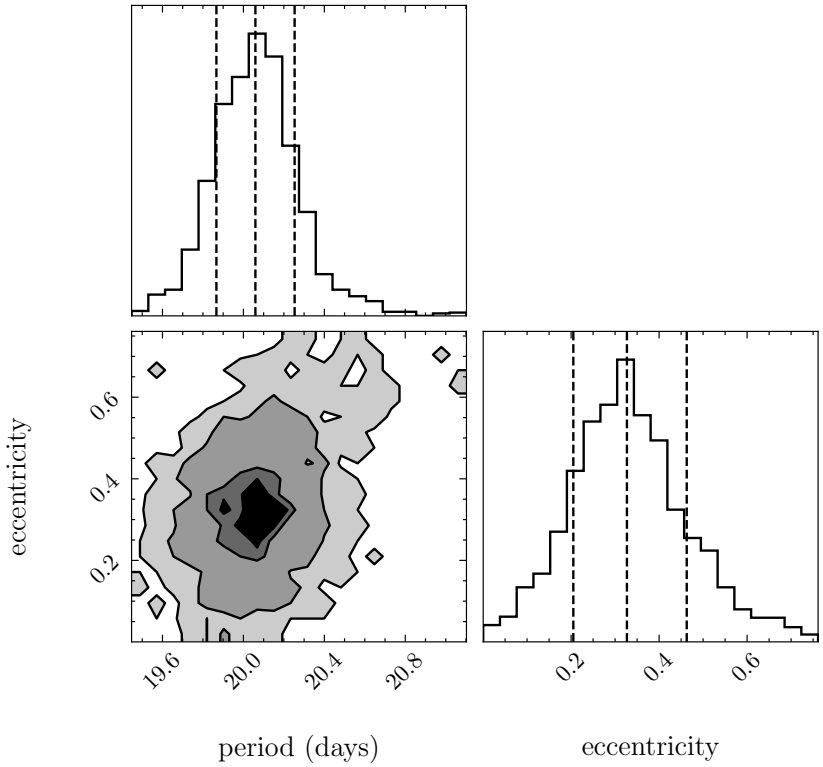

Figure A.16: Period: 20 days, Moon Mass: 120 $M_{\oplus}$, Noise= 250 m/s

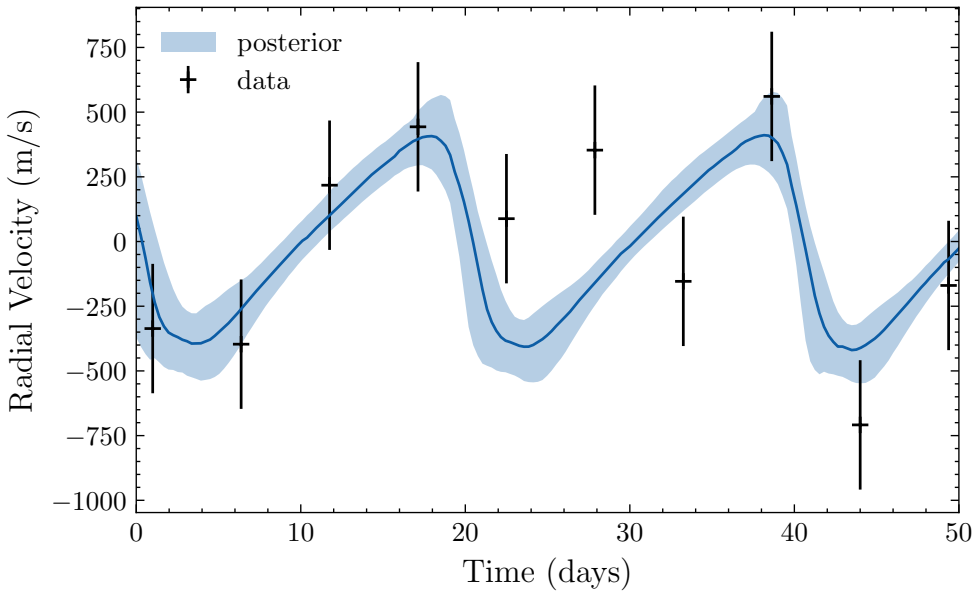

Figure A.17: Period: 20 days, Moon Mass: 90 $M_{\oplus}$, Noise= 250 m/s

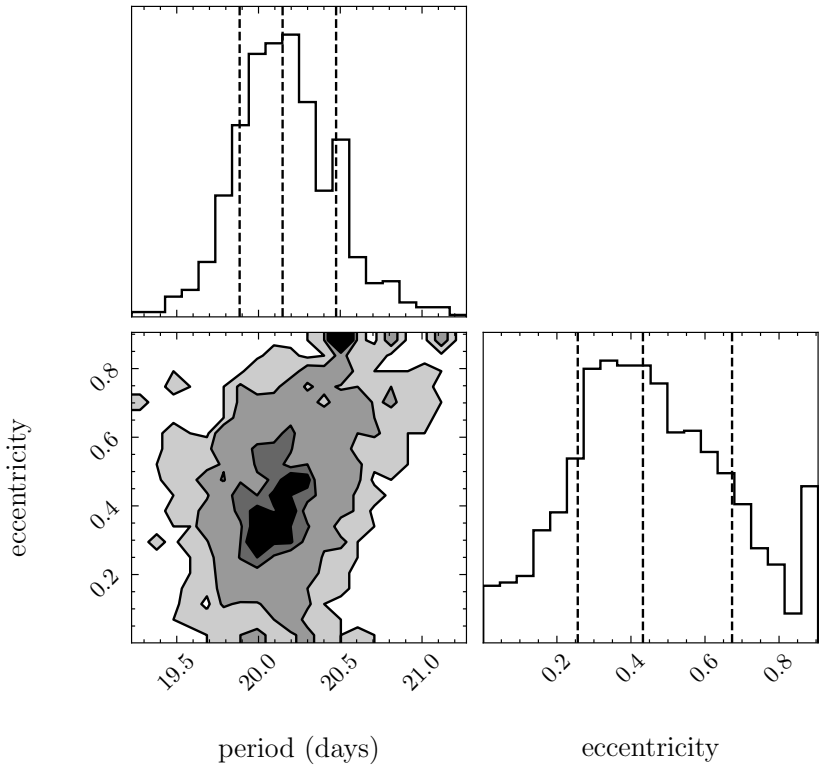

Figure A.18: Period: 20 days, Moon Mass: 90 $M_{\oplus}$, Noise= 250 m/s

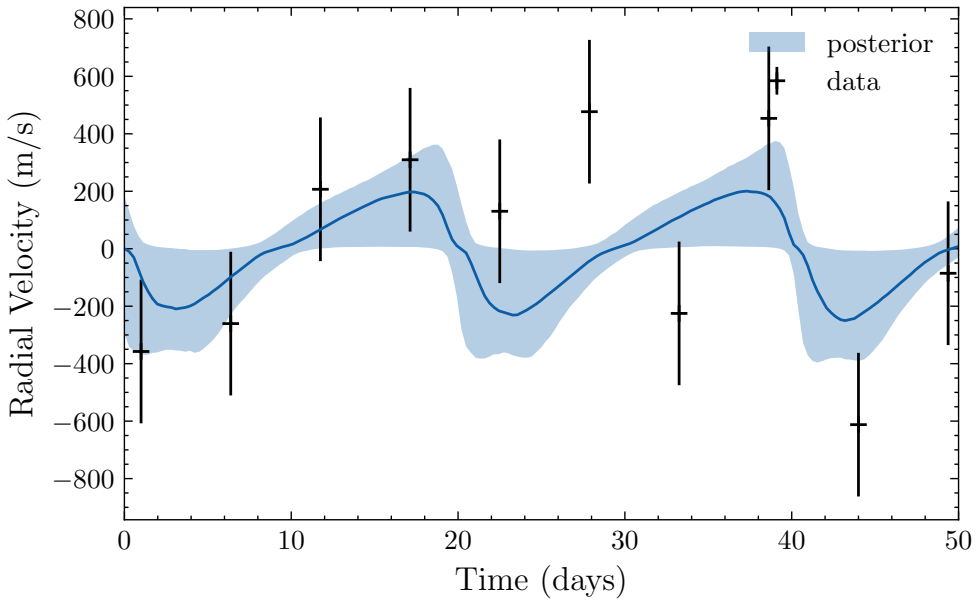

Figure A.19: Period: 20 days, Moon Mass: 60 $M_{\oplus}$, Noise= 250 m/s

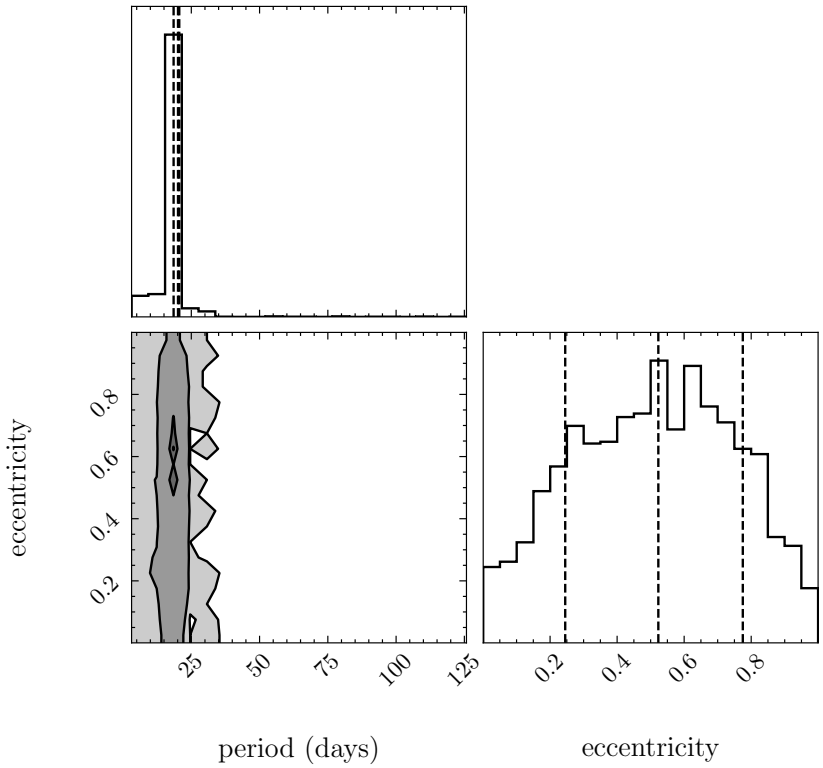

Figure A.20: Period: 20 days, Moon Mass: 60 $M_{\oplus}$, Noise= 250 m/s

Bibliography

Agol, Eric, Rodrigo Luger, and Daniel Foreman-Mackey (Mar. 2020). "Analytic Planetary Transit Light Curves and Derivatives for Stars with Polynomial Limb Darkening". In: *The Astronomical Journal* 159.3, p. 123. DOI: 10.3847/1538-3881/ab4fee.

Alibert, Y., O. Mousis, and W. Benz (Sept. 2005). "Modeling the Jovian subnebula. I. Thermodynamic conditions and migration of proto-satellites". In: *Astronomy & Astrophysics* 439.3, pp. 1205–1213. DOI: 10.1051/0004-6361:20052841. arXiv: astro-ph/0505367 [astro-ph].

Astropy Collaboration et al. (Oct. 2013). "Astropy: A community Python package for astronomy". In: *Astronomy & Astrophysics* 558, A33. DOI: 10.1051/0004-6361/201322068.

Astropy Collaboration et al. (Sept. 2018). "The Astropy Project: Building an Open-science Project and Status of the v2.0 Core Package". In: *The Astronomical Journal* 156, p. 123. DOI: 10.3847/1538-3881/aabc4f.

Bonnefoy, M. et al. (July 2014). "Physical and orbital properties of Beta Pictoris b". In: *Astronomy & Astrophysics* 567, p. L9. DOI: 10.1051/0004-6361/201424041. URL: https://doi.org/10.1051%2F0004-6361%2F201424041.

Chauvin, G. et al. (Oct. 2004). "A giant planet candidate near a young brown dwarf. Direct VLT/NACO observations using IR wavefront sensing". In: *Astronomy & Astrophysics* 425, pp. L29–L32. DOI: 10.1051/0004-6361:200400056. arXiv: astro-ph/0409323 [astro-ph].

Chauvin, G. et al. (June 2012). "Orbital characterization of the β Pictoris b giant planet". In: 542, A41, A41. DOI: 10.1051/0004-6361/201118346. arXiv: 1202.2655 [astro-ph.EP].

Currie, Thayne et al. (Oct. 2013). "A Combined Very Large Telescope and Gemini Study of the Atmosphere of the Directly Imaged Planet, β Pictoris b". In: *Astrophysical Journal* 776.1, 15, p. 15. DOI: 10.1088/0004-637X/776/1/15. arXiv: 1306.0610 [astro-ph.EP].

Czesla, Stefan et al. (June 2019). *PyA: Python astronomy-related packages*. ascl: 1906.010.

European South Observatory (n.d.). *Beta Pictoris as seen in infrared light - annotated*. visited on 23-12-2022. URL: https://www.eso.org/public/images/eso0842b/.

European Southern Observatory (n.d.[a]). *CRIRES+: The CRyogenic InfraRed Echelle Spectrograph Upgrade Project*. visited on 10-12-2022. URL: https://www.eso.org/sci/facilities/develop/instruments/crires_up.html.

— (n.d.[b]). *Object Observability*. visited on 11-12-2022. URL: https://www.eso.org/sci/observing/tools/calendar/observability.html.

— (n.d.[c]). *Paranal Observatory*. visited on 11-12-2022. URL: https://www.eso.org/public/teles-instr/paranal-observatory/.

Exoplanet Team (n.d.). *The Extrasolar Planets Encyclopaedia*. visited on 16-11-2022. URL: http://exoplanet.eu/.

Foreman-Mackey, Daniel (June 2016). "corner.py: Scatterplot matrices in Python". In: *The Journal of Open Source Software* 1.2, p. 24. DOI: 10.21105/joss.00024. URL: https://doi.org/10.21105/joss.00024.

Foreman-Mackey, Daniel, Rodrigo Luger, et al. (May 2021a). "exoplanet: Gradient-based probabilistic inference for exoplanet data & other astronomical time series". In: *arXiv e-prints*, arXiv:2105.01994, arXiv:2105.01994. arXiv: 2105.01994 [astro-ph.IM].

— (June 2021b). *exoplanet: Gradient-based probabilistic inference for exoplanet data & other astronomical time series*. Zenodo. Version 0.5.1. DOI: 10.5281/zenodo.1998447.

Foreman-Mackey, Daniel, Arjun Savel, et al. (June 2021). *exoplanet-dev/exoplanet v0.5.1*. DOI: 10.5281/zenodo.1998447. URL: https://doi.org/10.5281/zenodo.1998447.

Gilbert, Emily A. et al. (Sept. 2020). "The First Habitable-zone Earth-sized Planet from TESS. I. Validation of the TOI-700 System". In: *The Astronomical Journal* 160.3, 116, p. 116. DOI: 10.3847/1538-3881/aba4b2. arXiv: 2001.00952 [astro-ph.EP].

GRAVITY Collaboration et al. (Jan. 2020). "Peering into the formation history of β Pictoris b with VLTI/GRAVITY long-baseline interferometry". In: *Astronomy & Astrophysics* 633, A110, A110. DOI: 10.1051/0004-6361/201936898. arXiv: 1912.04651 [astro-ph.EP].

Heller, R. (Apr. 2016). "Transits of extrasolar moons around luminous giant planets". In: *Astronomy & Astrophysics* 588, A34, A34. DOI: 10.1051/0004-6361/201527496. arXiv: 1603.00174 [astro-ph.EP].

Heller, R. and R. Barnes (Apr. 2015). "Runaway greenhouse effect on exomoons due to irradiation from hot, young giant planets". In: *International Journal of Astrobiology* 14.2, pp. 335–343. DOI: 10.1017/S1473550413000463. arXiv: 1311.0292 [astro-ph.EP].

Heller, René (Sept. 2020). "Astrophysical Simulations and Data Analyses on the Formation, Detection, and Habitability of Moons Around Extrasolar Planets". In: *arXiv e-prints*, arXiv:2009.01881, arXiv:2009.01881. arXiv: 2009.01881 [astro-ph.EP].

Heller, René and Rory Barnes (Jan. 2013). "Exomoon Habitability Constrained by Illumination and Tidal Heating". In: *Astrobiology* 13.1, pp. 18–46. DOI: 10.1089/ast.2012.0859. arXiv: 1209.5323 [astro-ph.EP].

Kipping, D. M. (Nov. 2013). "Efficient, uninformative sampling of limb darkening coefficients for two-parameter laws". In: *Monthly Notices of the RAS* 435, pp. 2152–2160. DOI: 10.1093/mnras/stt1435.

Kipping, David et al. (June 2022). "An Exomoon Survey of 70 Cool Giants and the New Candidate Kepler-1708 b-i". In: *Bulletin of the American Astronomical Society*. Vol. 54, 504.04, p. 504.04.

Kipping, David M. (Jan. 2009a). "Transit timing effects due to an exomoon". In: *Monthly Notices of the RAS* 392.1, pp. 181–189. DOI: 10.1111/j.1365-2966.2008.13999.x. arXiv: 0810.2243 [astro-ph].

— (July 2009b). "Transit timing effects due to an exomoon - II". In: *Monthly Notices of the RAS* 396.3, pp. 1797–1804. DOI: 10.1111/j.1365-2966.2009.14869.x. arXiv: 0904.2565 [astro-ph.EP].

Kumar, Ravin et al. (2019). "ArviZ a unified library for exploratory analysis of Bayesian models in Python". In: *The Journal of Open Source Software*. DOI: 10.21105/joss.01143. URL: http://joss.theoj.org/papers/10.21105/joss.01143.

Lacour, S. et al. (Oct. 2021). "The mass of β Pictoris c from β Pictoris b orbital motion". In: *Astronomy & Astrophysics* 654, L2, p. L2. DOI: 10.1051/0004-6361/202141889. arXiv: 2109.10671 [astro-ph.EP].

Lagrange, A. -M. et al. (Jan. 2019). "Post-conjunction detection of β Pictoris b with VLT/SPHERE". In: *Astronomy & Astrophysics* 621, L8, p. L8. DOI: 10.1051/0004-6361/201834302. arXiv: 1809.08354 [astro-ph.EP].

Luger, R. et al. (Feb. 2019). "starry: Analytic Occultation Light Curves". In: *The Astronomical Journal* 157, p. 64. DOI: 10.3847/1538-3881/aae8e5.

Luger, Rodrigo, Eric Agol, et al. (Feb. 2019). "starry: Analytic Occultation Light Curves". In: *The Astronomical Journal* 157.2, 64, p. 64. DOI: 10.3847/1538-3881/aae8e5. arXiv: 1810.06559 [astro-ph.IM].

Luger, Rodrigo, Megan Bedell, et al. (Mar. 2019). "TESS Photometric Mapping of a Terrestrial Planet in the Habitable Zone: Detection of Clouds, Oceans, and Continents". In: *arXiv e-prints*, arXiv:1903.12182, arXiv:1903.12182. arXiv: 1903.12182 [astro-ph.EP].

Luger, Rodrigo, Daniel Foreman-Mackey, and Christina Hedges (Sept. 2021a). "Mapping Stellar Surfaces. II. An Interpretable Gaussian Process Model

for Light Curves". In: *The Astronomical Journal* 162.3, 124, p. 124. DOI: 10.3847/1538-3881/abfdb9. arXiv: 2102.01697 [astro-ph.SR].

Luger, Rodrigo, Daniel Foreman-Mackey, and Christina Hedges (July 2021b). "starry_process: Interpretable Gaussian processes for stellar light curves". In: *The Journal of Open Source Software* 6.63, 3071, p. 3071. DOI: 10.21105/joss.03071. arXiv: 2102.01774 [astro-ph.SR].

Luger, Rodrigo, Daniel Foreman-Mackey, Christina Hedges, and David W. Hogg (Sept. 2021). "Mapping Stellar Surfaces. I. Degeneracies in the Rotational Light-curve Problem". In: *The Astronomical Journal* 162.3, 123, p. 123. DOI: 10.3847/1538-3881/abfdb8. arXiv: 2102.00007 [astro-ph.SR].

Mohanty, Subhanjoy et al. (Mar. 2007). "The Planetary Mass Companion 2MASS 1207-3932B: Temperature, Mass, and Evidence for an Edge-on Disk". In: *Astrophysical Journal* 657.2, pp. 1064–1091. DOI: 10.1086/510877. arXiv: astro-ph/0610550 [astro-ph].

Nielsen, Eric L. et al. (Feb. 2020). "The Gemini Planet Imager Exoplanet Survey: Dynamical Mass of the Exoplanet β Pictoris b from Combined Direct Imaging and Astrometry". In: *The Astronomical Journal* 159.2, 71, p. 71. DOI: 10.3847/1538-3881/ab5b92. arXiv: 1911.11273 [astro-ph.EP].

Ruffio, Jean-Baptiste et al. (Nov. 2019). "Radial Velocity Measurements of HR 8799 b and c with Medium Resolution Spectroscopy". In: *The Astronomical Journal* 158.5, 200, p. 200. DOI: 10.3847/1538-3881/ab4594. arXiv: 1909.07571 [astro-ph.EP].

Salvatier, John, Thomas V Wiecki, and Christopher Fonnesbeck (2016a). "Probabilistic programming in Python using PyMC3". In: *PeerJ Computer Science* 2, e55.

— (2016b). "Probabilistic programming in Python using PyMC3". In: *PeerJ Computer Science* 2, e55.

Stolker, Tomas (2021). *Data reduction pipeline for VLT/CRIRES+*. URL: https://pycrires.readthedocs.io/.

Teachey, A., D. M. Kipping, and A. R. Schmitt (Jan. 2018). "HEK. VI. On the Dearth of Galilean Analogs in Kepler, and the Exomoon Candidate Kepler-1625b I". In: *The Astronomical Journal* 155.1, 36, p. 36. DOI: 10.3847/1538-3881/aa93f2. arXiv: 1707.08563 [astro-ph.EP].

Theano Development Team (May 2016). "Theano: A Python framework for fast computation of mathematical expressions". In: *arXiv e-prints* abs/1605.02688. URL: http://arxiv.org/abs/1605.02688.

Triaud, Amaury H. M. J. (2018). "The Rossiter–McLaughlin Effect in Exoplanet Research". In: pp. 1375–1401. DOI: 10.1007/978-3-319-55333-7_2. URL: https://doi.org/10.1007%5C%2F978-3-319-55333-7_2.

Virtanen, Pauli et al. (2020). "SciPy 1.0: Fundamental Algorithms for Scientific Computing in Python". In: *Nature Methods* 17, pp. 261–272. DOI: 10.1038/s41592-019-0686-2.

Wolszczan, A. and D. A. Frail (Jan. 1992). "A planetary system around the millisecond pulsar PSR1257 + 12". In: *Nature* 355.6356, pp. 145–147. DOI: 10.1038/355145a0.